Journal of Structural Geology xxx (xxxx) 105563

Contents lists available at ScienceDirect

Journal of Structural Geology

journal homepage: www.elsevier.com/locate/jsg

Effects of pre-existing fractures on dike propagation: new insights from field data and numerical modelling

A. Luppino [a, *], F.L. Bonali [a, b], A. Gudmundsson [c], A. Tibaldi [a, b]

[a] University of Milan Bicocca, Milan, Italy
[b] CRUST – Interuniversity Centre for 3D Seismotectonics with Territorial Applications, Chieti, Italy
[c] Royal Holloway University, London, UK

ARTICLE INFO

Keywords:
Mt Etna
Dike
Pre-existing fractures
Stress field
Numerical models

ABSTRACT

To better understand the conditions and mechanisms under which dikes interact with pre-existing vertical fractures, we analyzed the fracture swarm and volcanic vents developed during the 1947 eruption (North-East Rift, Etna), and reconstructed the pre-1947 fracture field by historical aerial photos. Then we developed Finite Element Method numerical models, varying the number, spacing, width and vertical and lateral distance of pre-existing fractures with respect to a dike, as well as the dike overpressure. Although in general the 1947 dike followed the path of a previous dike, at a more detailed scale the 1947 vents are shifted up to 11 m laterally with respect to the nearest pre-existing fracture. In areas where few fractures were already present, a significant number of new fractures developed during the 1947 event, whereas if several fractures pre-existed, a few new ones formed. In the case of a pre-existent single fracture, numerical models suggest two scenarios: nucleation of a new fracture bending toward the pre-existing one, possibly followed by dike deflection, or the vertical propagation of the dike. The latter is facilitated by close pre-existing fractures, because dike/fracture interaction enhances tensile stress above the dike tip. This stress increase is sensitive to horizontal fracture spacing, dike/fracture depth difference, and dike overpressure. Stress concentration towards the dike tip and fracture base means a lower probability of new fractures formation at the surface if pre-existing fractures are already widespread. A dike located nearby, or in the middle, of already existing fractures, receives a stress "booster" enhancing its probability of further propagation.

1. Introduction

The primary way by which basaltic magmas travel through the Earth's crust is through vertical to sub-vertical fractures filled with magma, known as dikes. Dikes mostly intrude perpendicular to the least principal stress (σ_3) (Anderson, 1951; Hubbert and Willis, 1957). This can occur by opening a new tensile, planar fracture thanks to the magma overpressure, which follows a plane containing the greatest compressive (σ_1) and intermediate (σ_2) stress (Anderson, 1951). These are referred to as self-propagating dike-fractures (Lister and Kerr, 1991; Spence and Turcotte, 1985) or, alternatively, as fluid-driven fractures or hydrofractures (Gudmundsson, 2022). Additionally, dikes can propagate by expanding pre-existing fractures, particularly columnar joints, that are oriented favorably in relation to the σ_3 and σ_1 (Gudmundsson, 1984, 2022; Delaney et al., 1986; Baer et al., 1994). A variety of research grounded in field observations of dikes and analogue models indicates that the propagation of these features can be more complicated. This complexity may arise from several factors, including a shearing component in the vicinity (the process zone, i.e. the walls and at the tip) of a propagating dike (Stephens et al., 2018; Gudmundsson, 2022), interactions with fractures inherited by previous phases of deformation (Spacapan et al., 2016; Poppe et al., 2020; Pedicini et al., 2023, 2025), the characteristics of the magma that intrudes (Schmiedel et al., 2021), topography (Le Corvec et al., 2013; Maccaferri et al., 2015; Harp and Valentine, 2018; Gaete et al., 2019; Muller et al., 2001; Watanabe et al., 2002; Bonali et al., 2024a; Tibaldi et al., 2025), fracture dimensions (Maccaferri et al., 2019) and variations in the material properties of the surrounding rock, such as the presence of different lithotypes (Drymoni et al., 2021; Gudmundsson, 2022; Corti et al., 2023; Greiner et al., 2025).

However, models that are commonly employed to understand the constraints of diking at depth, frequently depict dikes as elastic dislocations that open within a uniform, often fully elastic medium – an elastic half-space (e.g. Okada, 1985, 1992; Wright et al., 2006; Wauthier et al.,

* Corresponding author.
E-mail address: a.luppino6@campus.unimib.it (A. Luppino).

https://doi.org/10.1016/j.jsg.2025.105563
Received 6 September 2025; Received in revised form 14 October 2025; Accepted 20 October 2025
0191-8141/

2012; Sigmundsson et al., 2015). In reality, anisotropy due to layering and fracturing is a fundamental aspect to keep into account. Various types of geologic/geodynamic settings can exhibit different intensities and forms of fracturing. For instance, vertical fractures or open fissures produced by tectonic, magmatic or gravity forces, cooling joints associated to lava successions, and normal faults with different degrees of inclination also produced under different processes, represent major mechanical discontinuities in the host rocks (e.g. Bonali et al., 2024a; Tibaldi et al., 2025). On one side, field researches on dikes found in eroded volcanoes suggest that magma propagation pathways in the upper crust can be guided by pre-existing discontinuities, such as joints and fault zones (Gudmundsson, 1984, 2022; Delaney et al., 1986; Baer et al., 1994; Jolly and Sanderson, 1997; Bonali et al., 2012; Tibaldi et al., 2013; Martínez-Poza et al., 2014; Browning and Gudmundsson, 2015; Greiner et al., 2023). On the other side, some theoretical studies argue that there is little mechanical advantage in intruding along pre-existing fractures (Lister and Kerr, 1991) and dike propagation is not influenced by pre-existing mechanical discontinuities (Rubin, 1993, 1995). Despite extensive research over the years into the conditions under which dikes interact with pre-existing fractures, the underlying mechanisms remain unclear. Gaining a deeper understanding of how dikes and fractures interact could refine our knowledge of potential propagation paths and eruption sites during volcanic unrest, thereby aiding in hazard assessments.

In order to contribute to a better understanding of the interaction between propagating dikes and existing fractures in the host rock, we developed a series of numerical models anchored to field geological and structural data. Field data are of paramount importance to construct reliable models and validate them, and understanding the past processes as observed in the field becomes crucial for anticipating future processes. One problem with using field data for our purpose is because in highly dynamic environments, like active volcanic regions, the landscape can be dramatically altered within short periods. As a consequence, it may be difficult to find relevant field data on the fracture pattern pre-existing to a new dike-fed eruption. Here, we used key examples from the volcanotectonic North-East Rift, lying on the northern flank of Mt. Etna, Italy. In this context, structural discontinuities at the surface can manifest as faults, fissures or fractures, which accumulate over the time with successive magma injections, allowing investigating their impact on dike propagation and the development of new fractures. We used field data partially published in Tibaldi et al. (2025), on the fracture pattern pre- and post-diking event of 1947 on Mt. Etna, coupled with new field data and a series of new Finite Element Method (FEM) numerical models, mimicking the various possible fracture conditions with respect to successive dike intrusions.

2. Geological background

Mt. Etna, located at the convergent boundary between the African and Eurasian plates, is characterized by a complex geodynamic framework driven by both regional tectonic forces and local magmatic and gravity processes. The western and northern flanks of the volcano experience a compressive stress regime at crustal depths, linked to the Apennine–Maghrebian thrust-and-fold belt. This compression is accommodated by shallow thrusting and folding (De Guidi et al., 2015; Tringali et al., 2023). By contrast, the eastern and southern flanks of Mt. Etna are characterized by persistent, radial sliding towards the sea (Fig. 1A), driven by gravitational spreading and magmatic intrusions (Borgia et al., 1992; Rust and Neri, 1996; Tibaldi and Groppelli, 2002). This flank instability is marked by the activation of several faults, including the Timpe Fault System (TFS in Fig. 1A) in the southeast and the Pernicana Fault System (PFS in Fig. 1A) to the northeast. In particular, the main fault related to this system, the Pernicana Fault, is dominated by left-lateral strike-slip motions that reaches about 1.5–2.7 cm/yr (Neri et al., 2004) on its western segment, whereas the newly mapped eastern segment moves at roughly 1–1.9 cm/yr (Groppelli and Tibaldi, 1999). The

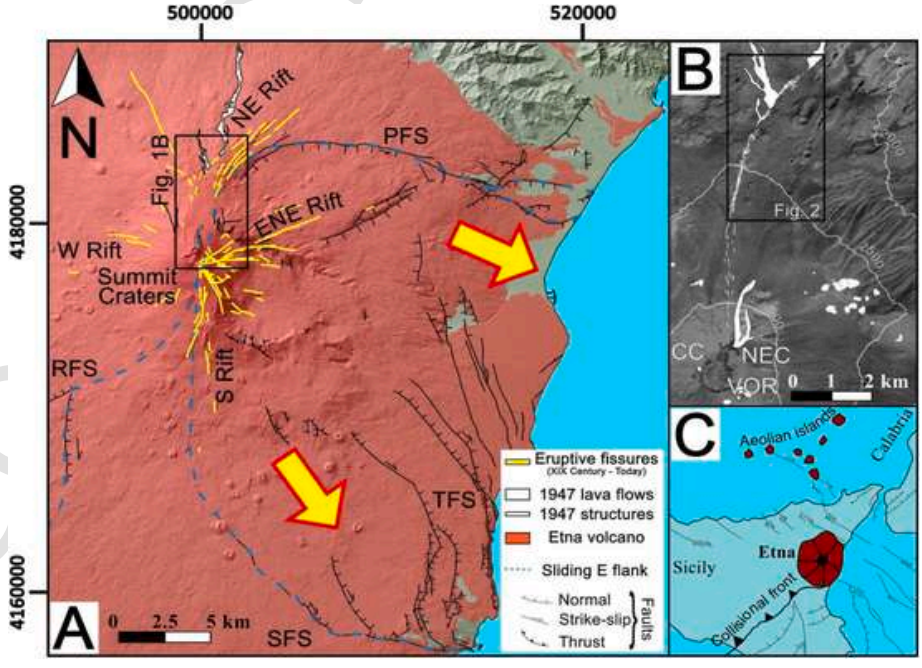

Fig. 1. (A) Volcanotectonic framework of Mt. Etna, showing the distribution of rift systems (NE, ENE, S, and W Rifts) relative to the summit craters, alongside major fault systems, including the Pernicana Fault System (PFS), Timpe Fault System (TFS), South Fault System (SFS), and Ragalna Fault System (RFS). (B) 1954 Orthomosaic of the upper part of Mt. Etna, illustrating the 1947 eruption lavas (white) and its associated structures. The box indicates the studied area of Fig. 2. CC = Central Crater, NEC = North-East Crater, VOR = Voragine crater. (C) Regional setting of Mt. Etna, with main regional faults. Modified after Gambino et al., (2022) and Drymoni et al., (2023). Reference system: WGS84 - UTM33N. Etna volcano boundaries from Branca et al., (2011) and faults from Azzaro et al., (2012). DEM in A from Regione Sicilia - volo ATA 2012 2013 http://www.sitr.regione.sicilia.it.

accompanying vertical component is much smaller, only a few millimeters per year, and both components can increase sharply during seismic or eruptive crises: during the 2002–2003 eruption, offsets of ~1 m were measured in the western PFS and ~0.1 m in the eastern PFS (Neri et al., 2004). The interaction between these fault systems, magmatic intrusions, and the volcano's eruptive activity, has led to the formation of four primary structural zones of weakness, known as rift sectors (e.g. Rittman, 1973; Kieffer, 1975; Garduno et al., 1997), defined by their orientation and location: the North-East, East-Northeast, South, and Western rifts (respectively NER, ENER, SR and WR, Fig. 1A).

The ongoing frequent activity of Mt. Etna is also marked by the significant morphological and structural changes that occurred, over the last century, in the summit sector of the volcano, marked by the formation and evolution of multiple craters. The North-East Crater (NEC, Fig. 1A) emerged in 1911 AD as a sub-terminal vent of the pre-existing Central Crater (CC). Subsequently, the Voragine (VOR) and Bocca Nuova (BN) craters formed within the CC following partial collapses in 1945 and 1968 as pit craters, respectively. In 1971, the South-East Crater (SEC) developed but was covered by the New South-East Crater (NSEC), which initiated in 2011 and continues to be a focal point of eruptive activity (Branca et al., 2011; Proietti et al., 2023).

From January 1947, both the summit craters present at the time, the NEC and the CC within the VOR inside, returned in activity after a period of quiescence. This activity, whose peaks were described as lava fountains from Silvestri (1949) and later as sub-plinians by Branca and Del Carlo, (2005) occurred in the NEC on 5th and 6th of February. A few days later, on the 10th of February, the NEC produced a paroxysmal episode with lava fountains 600 m high and later, on the 16th day of the same month, the CC did the same. In addition, the collapse of the VOR that occurred in January increased considerably the diameter of this crater, from about 5 m to over 200 m (Silvestri, 1949). According to Silvestri (1949), these episodes could have obstructed the central conduct, blocking the new vertical rise of magma and leading it to propagate laterally toward the NEC and then to the NER, with the lateral eruption that started on February 24th. In less than a day, the 1947 dike propagated for more than 6 km (La Sicilia, 26 February 1947; Ponte, 1947, 1948; Silvestri, 1949; Tibaldi et al., 2025) along the northwestern portion of the NER, following a pre-existing series of fractures (Fig. 2, Tibaldi et al., 2025).

The series of pre-existing fractures that preceded the 1947 dike intrusion were essentially present on few lavas related to historical eruptions. Using historical photographs and cross-referencing ancient documents and maps, Tibaldi et al. (2025) were able to define all the lavas

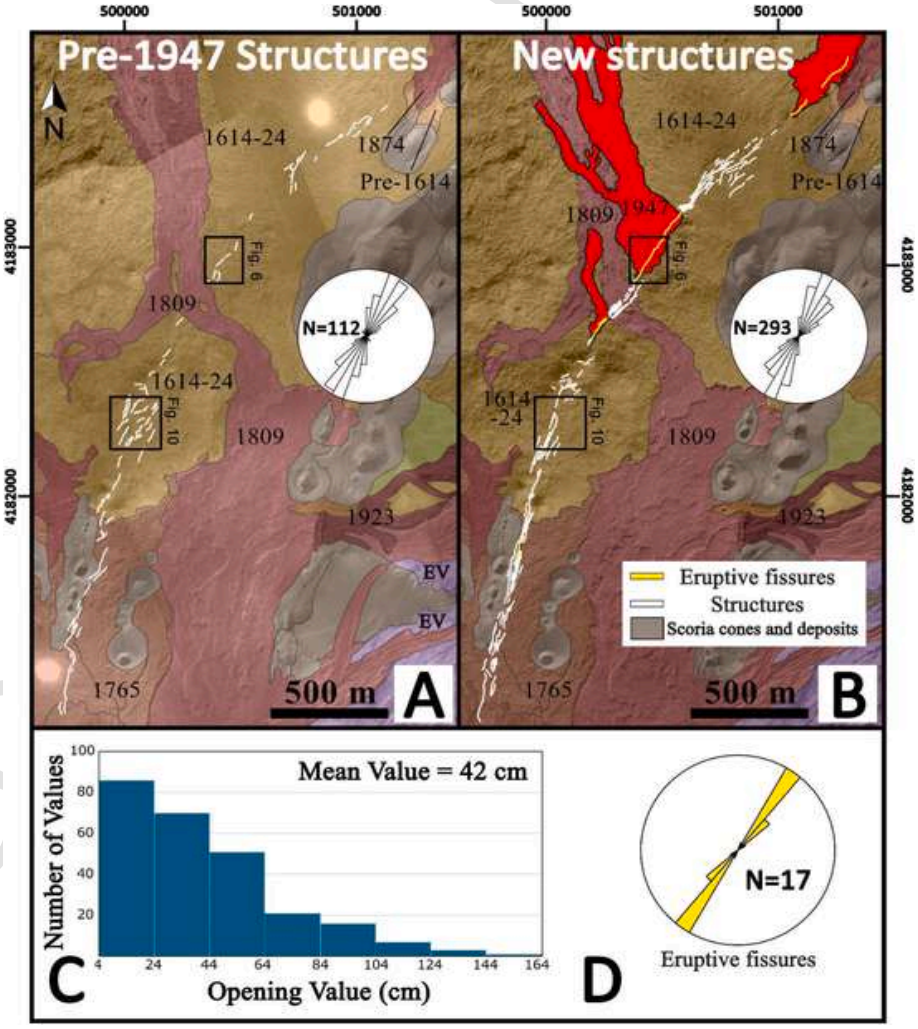

Fig. 2. Geological map of the year 1932 (A) and 1954 (B) with the pre- and syn-1947 structures highlighted. Reference system: UTM33-WGS84. Modified from Tibaldi et al. (2025). Ages of historical lavas are shown. EV = Ellittico volcano lavas. The diagram in C shows amounts of dilation measured by 255 Piercing Points at pre-existing and newly formed structures over the 1947 dike's path. The rose diagram in A gives strike values of pre-1947 fractures, and in C of 1947 fractures. D shows the strike of the 1947 eruptive fissures. OMs and DEMs obtained by photogrammetric elaboration of 1932 (A) and 1954 (B) aerial photos.

and scoria cones encountered (surficially) by the 1947 dike. This part is essential for our numerical model building in order to approximate reality as closely as possible and create reliable case scenarios.

In order of time, the first lavas crossed by the 1947 dike are related to the 1614-24 Eruption, probably the longest in historical time at Mt. Etna (Branca et al., 2011). During this event, an area of over 21 km^2 was covered by 1–2 km^3 of lava (Guest et al., 1984). A peculiarity of this lava flow, which facilitates its mapping, is the presence of plagioclase phenocrystals (the so-called "Cicirara" lava, Branca et al., 2011; Pappalardo et al., 2017). Other deposits crossed by the 1947 features are those produced by the 1809 eruption. This latter event consisted in a main eruptive fissure that extended for 4250 m from the summit CC to 1300 m a.s.l., together with a smaller one that extended for 1200 m nearly half of a kilometer north of the first one (Geshi and Neri, 2014).

3. Methodologies

The study of the effects of pre-existing structures on dike propagation and dike-induced deformations was made through a multidisciplinary approach that consisted, first of all, in a detailed assessment of the distribution of volcanic rocks and structures previous and syn-to the 1947 event, based on the data of Tibaldi et al. (2025). These were completed by further studies in key sites along the 1947 fracture system through new field mapping at a higher detail. This was necessary to create a robust data input of field truth for the successive numerical modelling.

3.1. Field mapping

The further mapping of surface features associated with, and pre-existing to, the 1947 eruption, was conducted in the field and using two orthomosaics (OMs) derived from photogrammetric processing of historical aerial photographs captured in 1932 and 1954. These remotely-sensed datasets, selected to represent the temporal windows immediately before and after the eruption, were processed using Agisoft Metashape®, employing imagery sourced from the Istituto Geografico Militare (IGM, https://igmi.org/). In particular, our work consisted in an increase of detail, using 150 Ground Control Points (GCPs), despite the 22 GCPs used in Tibaldi et al. (2025), to locate the same Dense Point Clouds. In addition, in the present work we introduced the use of Digital Elevation Models (DEMs) to obtain high-resolution mapping. The derived DEMs and OMs all had resolutions better than 30 cm/pixel. All the structures from the two OMs were then mapped and classified into pre-existing (all the structures present in the 1932 OM, Fig. 2A) and into newly formed (1954 OM, Fig. 2B) structures. The mapping was checked and completed by field and immersive virtual surveys (e.g. Antoniou et al., 2020; Tibaldi et al., 2021; Bonali et al., 2024b), including the distinction between open tension fractures, faults, geologic deposits, and eruptive vents (Fig. 3) published in Tibaldi et al. (2025). Opening values calculated by Piercing Points (PP) (for more details see Tibaldi et al., 2025) allowed us to calculate a mean opening value of the structures (Fig. 2C), useful for the numerical modelling processes.

3.2. Numerical modelling

The overall aim of our numerical models is to investigate the distribution and orientation of stress around the tip of a propagating dike, exploring possible interactions between different geometric combinations of existing fractures and a dike. With the term fractures, here we include both open tension fractures and faults. The aim is to explore the effects of the existing fractures in modifying the driving stresses at the tip of the propagating dike, thereby affecting its chances of further propagation or, alternatively, arrest. Our numerical models were designed with the Finite Element Methods (FEM) software COMSOL Multiphysics® starting from the field case studies. In particular, we investigated different features that could have influenced the arrest or the propagation of the 1947 dike, such as: *i)* one single pre-existing fracture, *ii)* effects of an increasing number of pre-existing fractures, *iii)* rising of the dike toward the surface, iv) dikes with different overpressure, and v) different fracture spacing.

3.2.1. Geometry and scaling

Our numerical analysis was done in a 2D static elastic setting, considering key cross-sections orthogonal to the fractures and to the direction of the dike. To emulate the conditions of the considered volcanic region, we built a base set-up where features such as pre-existing fractures and dikes were implemented. We considered a 500 × 500 m box (Fig. 4A) where a single-strata host rock was assumed to simplify the modeling framework in agreement with previous work (Gudmundsson, 2011; Browning et al., 2021; Bonali et al., 2024a). Most of the surface deformation associated with the 1947 eruption is in fact superimposed upon the 1614–1624 lava flow. As detailed previously, the stratigraphy

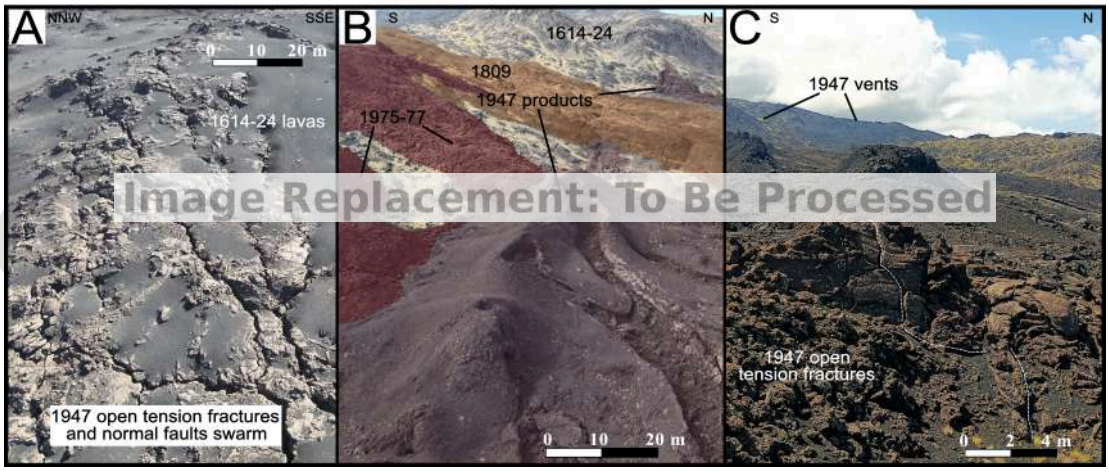

Fig. 3. Field surveys over the 1947 Etna eruption. (A) and (B) drone photos taken over open tension fractures and normal faults swarm and over the 1947 aligned vents respectively. (C) shows an open tension fracture induced by the 1947 dike's intrusion. Photo credits: Emanuela De Beni and Massimo Cantarero - INGV Osservatorio Etneo.

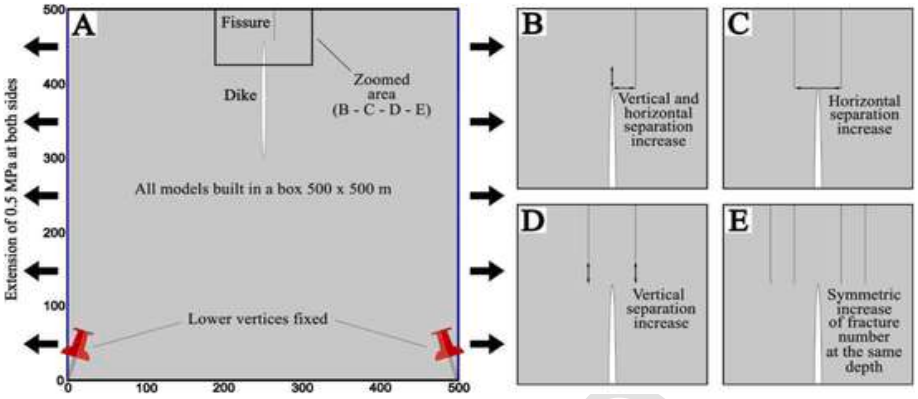

Fig. 4. Set-ups of our numerical models. Figure A shows the entire box with the arrows that indicate the extensional stress of 0.5 MPa for the two sides of the box and the pin that indicates the fixed constraints to avoid deformation after the numerical model computing. (B) Set-ups with the increase of the vertical and horizontal separation between dike and a single pre-existing fracture. (C) Increase of the horizontal separation between dike and two pre-existing fractures. (D) increase of the vertical separation between dike and two pre-existing fractures. (E) increase in the number of symmetric pre-existing fractures.

beneath this lava flow remains poorly constrained due to the lack of vertical and deep outcrops. Nevertheless, based on prior assessments, we adopt a mean thickness of 50 m for the 1614–1624 lava flow above the vertical extent targeted by our numerical models. This evaluation was carried out by employing the formula of erupted Volume (V)/Area covered by lava (A), utilizing the lowest estimated value published by Guest et al. (1984) to ensure a conservative and robust approximation:

$$\frac{V}{A} = \frac{1\ km^3}{21\ km^3} = 0.0476\ km = 47.6\ m$$

To model the dike, we build an elliptical cavity inside the host rock with different semi-axes values according to the considered case study. In most experiments, we considered a X semi-axis of 1 m (a 2 m wide or thick dike) and a Y semi-axis of 75 m (a dike-segment 150 m long in vertical section, dip-dimension). In a series of experiments, we also modeled dikes with a thickness of 1 m and 3 m for comparison, as will be detailed below. Regarding the fractures inserted into our models, we mostly considered for comparison among the various models, an opening or aperture of 1 cm and a vertical attitude, while for comparison we've done a series of models with 43 cm of opening, based on field values. Finally, regarding tension fractures length, we modeled different values to compare the effect of a dike approaching at different depths.

3.2.2. Constraining parameters

In our setting, we gave material properties to each geometry built into our setting, all resumed in Table 1. For the host rock we considered an 11 GPa value as Young Modulus (E) obtained by laboratory tests from Pappalardo et al. (2017). Regarding the fractures, we considered a Young Modulus of 0.001 GPa as previously done by Drymoni et al. (2021) in fracture modelling by the same software. For Poisson values (ν) we considered for both features a value of 0.25.

To model the dike rising into the host rock, we considered an elliptical cavity inside the host rock (Grosfils, 2007) with an internal overpressure. The value of this overpressure, defined as a stress directed normally from the dike towards the surrounding material (Gudmundsson, 2011), was, calculated with the formula used by several works (Sneddon, 1946; Gudmundsson, 2011; Geshi et al., 2020; Drymoni et al., 2021) as follows:

$$P_0 = \frac{W\,E}{2\,(1-\nu^2)\,L} = \frac{2\ m\ *\ 11*10^9 Pa}{2\ (1-0.0625)\ 6000\ m} = \frac{22*10^9 Pa}{11250} = 2\ MP$$

where W is the dike thickness, E is the young modulus of the host rock, ν is the Poisson's ratio and L is the total (horizontal) length of the dike.

Table 1
Parameters used in the numerical models.

Element	Value
Box	
Dimensions	500 x 500 m
Extensional stress (tensile loading)	0.5 MPa
Host rock	
Young Modulus [E]	11 GPa
Poisson [ν]	0.25
Density [ρ]	2800 kg/m^3
Pre-existing fracture(s)	
Number	1, 2, 4, 6 and 8
Opening/aperture	1 cm, 42 cm
Vertical length	5, 10, 20, 30, 40, 50, 60 and 70 m
Young Modulus [E]	0.001 GPa
Poisson [ν]	0.25
Density [ρ]	2800 kg/m^3
Dike	
Overpressure	1, 2 and 3 MPa
Thickness (aperture, opening)	1, 2 and 3 m
Vertical length	150 m
Horizontal distance dike/fractures	1, 2, 5, 10, 20, 30, 40 and 50 m

Several studies on numerical modelling of dike intrusion report consistent overpressure values (e.g. Gudmundsson, 1986, 2011; Drymoni et al., 2020; Corti et al., 2023; Bonali et al., 2024a; Corti, 2024) typically ranging between 2 and 6 MPa. Therefore, our obtained value of 2 MPa can be considered reliable.

The purpose of this work is to provide sensitivity analysis strongly based on field data. For this reason, for the dike we considered different openings/apertures or thickness into our numerical models, ranging from 1 to 3 m, because these values are consistent with the thickness of outcropping dikes found a few hundred meters from the studied area, produced by the similar 1809 North-East Rift eruption, which range around 2 m (Geshi and Neri, 2014). Our values are also consistent with the thickness of dikes found in the Mt. Calanna (Valle del Bove, Mt. Etna), which range 1–3 m (Ferlito and Nicotra, 2010). As a consequence, reliable values of 1, 2 and 3 MPa in the numerical models have been used.

In addition, we applied an external stress taking into account the local dynamic conditions, in order to make modeling as realistic as possible. The external stresses here are governed by the coexistence of a WNW-ESE regional tectonic σ_3 (Monaco et al., 1997, 2005; Giacomoni et al., 2012; Gambino et al., 2022) and the seaward sliding of the Mt. Etna flank, which can contribute to producing the WNW-ESE extensional stress. For this reason, in all the models we added an external σ_3

oriented perpendicularly to the dike/fracture system. The extensional local stress value has been considered 0.5 MPa based on previous modelling carried out on the eastern Mt. Etna by Drymoni et al. (2023) who considered the amount of average seaward displacement of the flank. They used a range of values of 0.5–2 MPa, whereas we used their lower value since our studied area is not exactly on the margin of the unstable volcano flank (Fig. 1A), but lies along the northwestern part of the NER. Finally, we placed a fixed constraint on the bottom of the box to avoid a dissipation of the stress that could increase the dimension of the box.

3.2.3. Result plotting and stress measurement

The plotted parameters are the distribution of the magnitude of the tensile and von Mises stresses as colored surfaces, plus the orientation of the σ_1 and σ_3 as oriented arrows, by definition at 90° each other. In the models, where the σ1 disappears is because it was oriented perpendicularly to the plane analyzed in the 2D model, and thus we also plotted the σ_2. The analysis of the von Mises stress is more related to the possible occurrence of faults, which based on some of our models have a poor probability of occurrence or re-mobilization under the examined settings. For this reason, we excluded the von Mises stress from most of the figures, in order to concentrate on the tensile stress.

To evaluate more precisely the change in stress due to the presence of pre-existing structures, we measured the values of tensile stress (and von Mises stress where necessary) at the dike tip. This stress has been evaluated as an average of 9 measurements (white dots in Fig. 5) above the dike tip. Points are 0.5, 1, 1.5 m above the dike tip and −0.5, 0 and 0.5 m of horizontal distance from the dike.

4. Results

4.1. Role of a single fracture

4.1.1. Field data

Geological observations from field surveys, interpretation of OMs and historical aerial photographs show a remarkable coincidence of location of pre-1947 and 1947 fractures (Fig. 2), clearly indicating that the 1947 dike followed, in general, the previous fracture path. Moreover, the rose diagrams in Fig. 2A and B indicate the strict correspondence of pre-1947 and 1947 fracture strike. These field observations contribute to justify the settings used in the numerical models. The maps of Fig. 6 reveal that, in selected segments of the 1947 fissure system, eruptive vents systematically developed in correspondence with isolated pre-existing vertical fractures. The comparison between 1932

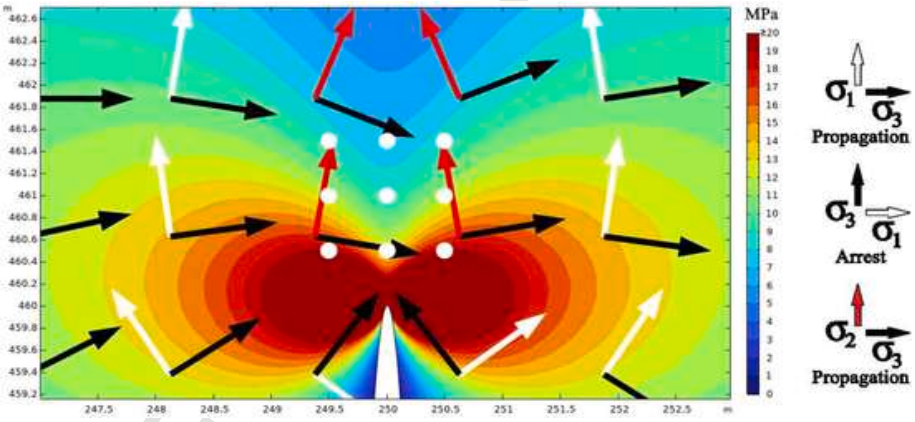

Fig. 5. Points of measurement of stress (white dots) used to obtain representative average values at the dike tip.

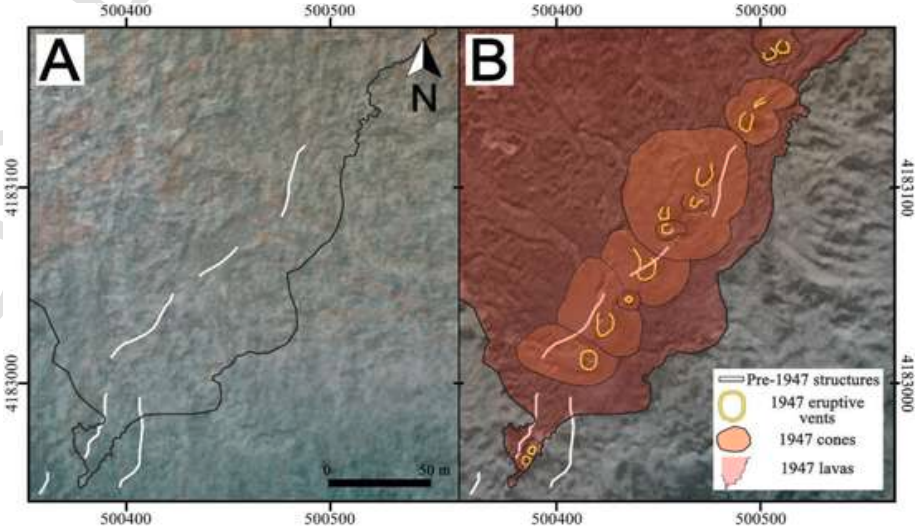

Fig. 6. A) 1932 OM shows the location of pre-existing fractures and B) 1954 OM where eruptive vents, cones and lavas of the 1947 eruption are shown. In both images, the lava contours and the pre-existing fractures are shown for comparison. Figures are made with OMs and DEMs in transparency. Location in Fig. 2.

and 1954 OM highlights that these inherited discontinuities can have interacted with magma ascent, thereby underscoring their mechanical control on surface vent localization. Despite this general aspect, at a higher detail of observation, the location of the eruptive vents is shifted laterally by a mean value of 7 m from the pre-existing nearest fracture. Among the 14 vents, only one is located exactly at the location of a previous fracture, 6 cones lie above an unfractured surface, and the remaining vents are shifted from 3 to 11 m with respect to the nearest fracture. The pre-1947 fractures are aligned with a N25°E trend, whereas the 1947 vents trend N35°E. This is shown also by the fact that in the southern part of Fig. 6B the fractures are west of the vents (apart one), whereas in the northern part, the fractures are east of the vents.

In order to develop numerical models that mimic not only vertical discontinuities but also open tension fractures, we used field data to quantify the dilation amount along the tension fractures cropping out along the 1947 system, plotted in the graph of Fig. 2C. The total number of measured dilation values, obtained by matching piercing points on the two sides of a fracture, is 255. The dilation values range from 4 cm to 161 cm, with an average amount of 42 cm. This average value has been used for the models (see supplementary materials).

4.1.2. Numerical data

A series of numerical simulations contribute to illuminating the influence of an isolated vertical tension fracture on dike propagation dynamics. We developed a series of models that consider a single fracture pre-existing during a dike intrusion, by varying the horizontal distance between the fracture and the dike and then varying the depth to the dike tip with respect to the base of the fracture (i.e. the lower fracture tip), for both cases calculating the tensile stress and the von Mises stress distribution. In another series of models, we used the same set-up for comparison, but then considered different opening values for the pre-existing vertical fracture and different overpressure values for the dike (see also Supplementary material).

At an overpressure of 2 MPa, when the dike tip is several tens of meters below the base of the fracture, there is no perturbation in the stress pattern. When the dike tip becomes closer to the depth of the fracture base, the stress pattern starts to change, with the maximum interaction with the fracture when the dike tip is at the same depth of the fracture base. Here we report this setting, which is the most meaningful, in Fig. 7. In the case of a dike almost aligned with an overlying pre-existing fracture (collinear, that is to say the fracture bottom is right above the dike tip) (Fig. 7A), the tensile stress is still quite symmetric and the area with the relative higher tensile magnitude prolongs into the fracture. In the case the dike is not collinear with the fracture (cases of Fig. 7B–E), the area of maximum tensile stress propagates horizontally from the dike tip to the fracture base. The stress pattern becomes highly asymmetric, with the development of areas of relatively higher stress to the side of the fracture where the dike is located. The calculation of the stress values at the dike tip, shows that the tensile stress increases significantly if a pre-existing fracture is present; this can be appreciated in the graph of Fig. 7, where the tensile stress value at the dike tip is around 20 MPa in the case of non-presence of fractures, whereas it increase up to a maximum of 35 MPa when the distance dike tip to the aligned fracture base is about 2 m. At greater distances, the tensile stress gradually decreases down to the value without the presence of a fracture, at a distance >30 m.

The von Mises stress has a general similar behavior, with the stress pattern that becomes asymmetric when the dike tip approaches the fracture base (Fig. 7G–K). A major difference with respect to the tensile stress, is that the von Mises stress tends to concentrate at the sides of the dike-fracture system, but also along the lower part of the fracture.

Compared with the case of no pre-existing fracture (Fig. 7F–L), it is noticed also that the pre-existing fracture enhances slightly the von Mises stress magnitude at the surface in the case of distances dike/fracture lower than 5–10 m, and increases more sensibly the tensile stress at the surface in the same distance range.

In regard to the orientation of the principal stresses, generally σ_1 is vertical and σ_3 is horizontal (Fig. 7F–8A), but when the dike tip approaches the base of the pre-existing structure, the local stress field is significantly perturbed (Fig. 8B). In the area between the dike tip and the fracture base, the σ_3 acquires a sub-horizontal attitude and dips towards the fracture (i.e. towards the right in the figure); the σ_1 also rotates assuming a dip towards the dike (i.e. towards the left). Moreover, a few meters above the dike tip, σ_1 interchanges with σ_2 and the latter is still oblique dipping towards the dike. In a situation where the two pre-existing fractures are located at the same distance from the dike (Fig. 8C), the σ_1 seems to be captured by the fractures in the first few meters. At slightly minor depths, a rotated pattern is evident, according to an increase of the tensile stress bands values.

Fig. 9 shows different vertical separation between a dike tip and a single pre-existing fracture. The horizontal distance between the dike and the fracture is 2 m for the tensile stress and 1 m for the von Mises shear stress, because these distances are those where there is the maximum increase of stress at the dike tip. With a dike overpressure of 2 MPa, the tensile stress at the dike tip starts to increase at a distance of 10 m below the fracture base (Fig. 9A), reaches the maximum value at the same depth of the fracture base, and gradually decreases to the initial value when the dike tip is about 35 m lower than the fracture base (Fig. 9E). The von Mises stress shows a similar pattern although the stress increase is lower.

Finally, we run the various models varying also the dike overpressure down to 1 MPa and up to 3 MPa, and assuming a pre-existing fissure with an opening of 42 cm instead of a fracture with width of 1 cm. Some examples of the results are reported in the supplementary materials (Fig. S1), where it can be observed that inserting a fissure does not modify the stress distribution with respect to a fracture. Varying the overpressure also does not change the general pattern apart from extending the areas of the largest stresses.

4.2. Role of multiple vertical fractures in dike propagation

4.2.1. Field data

Field evidence from the 1947 Etna eruption indicates that in areas where few fractures were already present (e.g. Fig. 10, lower part), a significant number of new fractures developed during the 1947 event. Conversely, where the density of pre-existing fractures was already high (e.g. Fig. 10, upper part), relatively few new fractures formed. More quantitatively, in the southern part of the pre-existing fracture swarm examined, there were 4 fractures; here, in 1947, 13 new fractures developed. By contrast, in the northern part there were 12 pre-existing fractures, and in 1947 only 5 new fractures developed here. This behavior has been observed in several parts of the whole, 6-km-long, 1947 fracture swarm.

Finally, in the key example of Fig. 10, the average trend of the pre-1947 fractures is N45°E, whereas the syn-1947 fractures strike on average N25°E.

4.2.2. Numerical data

In order to understand the process that, based on field data, suggests that the pre-existing fracture density may modulate both the mechanical response of the host rock and the evolution of the surface fracture network, we made a further series of numerical models. We investigated the mechanical implications of multiple vertical fractures, with a selection of models provided in Figs. 11–13, which explore how fracture number, spacing, and vertical positioning relative to the dike tip affect the local stress field.

Fig. 11 shows a series of models, each with a 2 MPa of dike overpressure, in which the dike tip is positioned at decreasing depths beneath the base of two vertical tension fractures, while the spacing be-

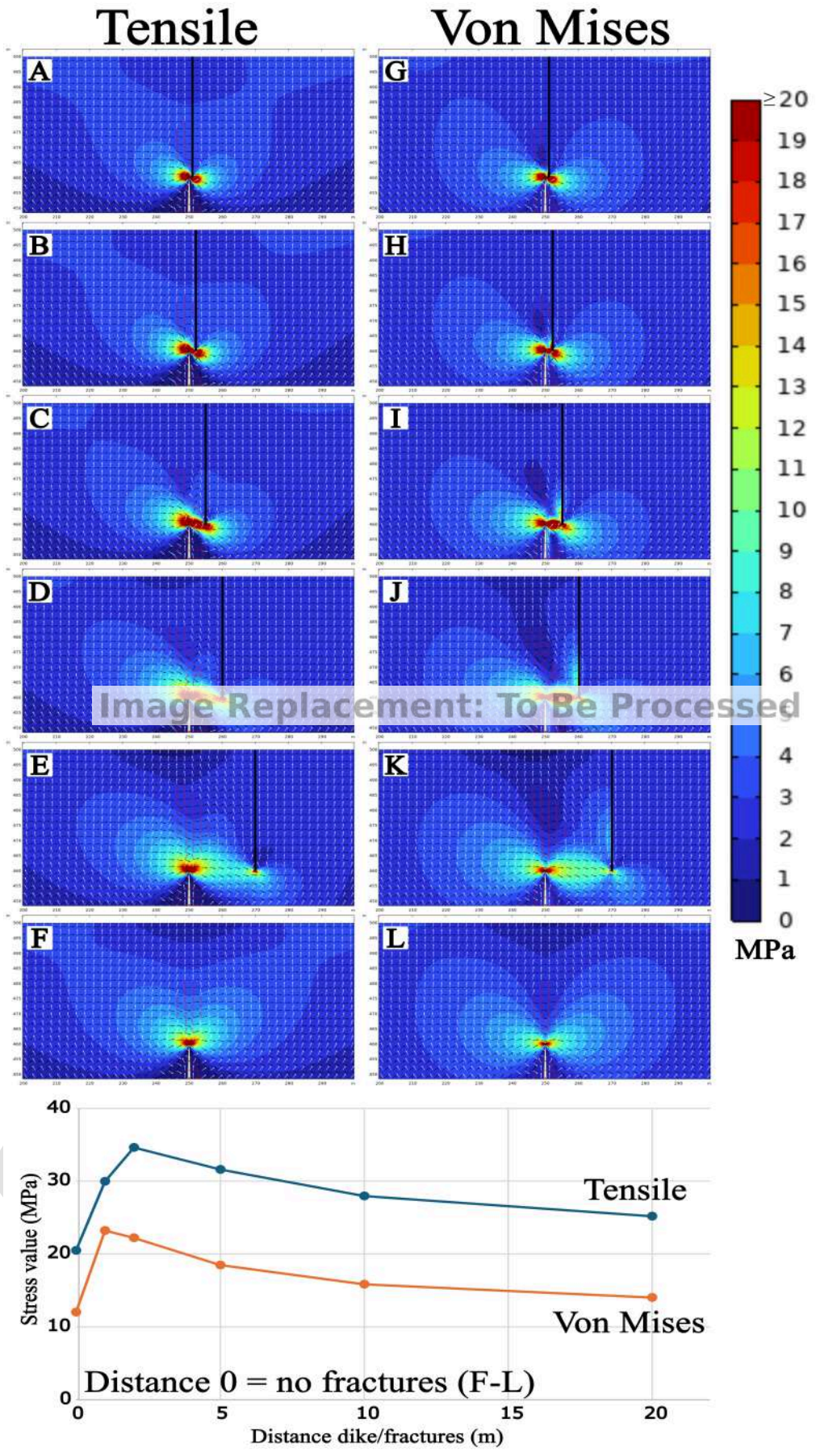
Tensile
Von Mises
A
B
C
D
E
F
G
H
I
J
K
L
≥20
19
18
17
16
15
14
13
12
11
10
9
8
7
6
5
4
3
2
1
0
MPa
Image Replacement: To Be Processed
40
30
20
10
0
Stress value (MPa)
Tensile
Von Mises
Distance 0 = no fractures (F-L)
0
5
10
15
20
Distance dike/fractures (m)

Fig. 7. *Numerical models A-E and G-K show the case of a dike near a pre-existing single vertical tension fracture, at different horizontal distances. The dike tip is maintained at 40 m of depth below the surface as the fracture base (lower tip). White arrows σ_1, black arrows σ_3, red arrows σ_2. Models F and L are without pre-existing fracture for comparison. The graph shows the stress value (Y-axis) measured at the dike tip in the case of no pre-existing fractures (0 value at X-axis) or with a pre-existing fracture at various distances from the dike (1 to 20 m).* (For interpretation of the references to color in this figure legend, the reader is referred to the Web version of this article.)

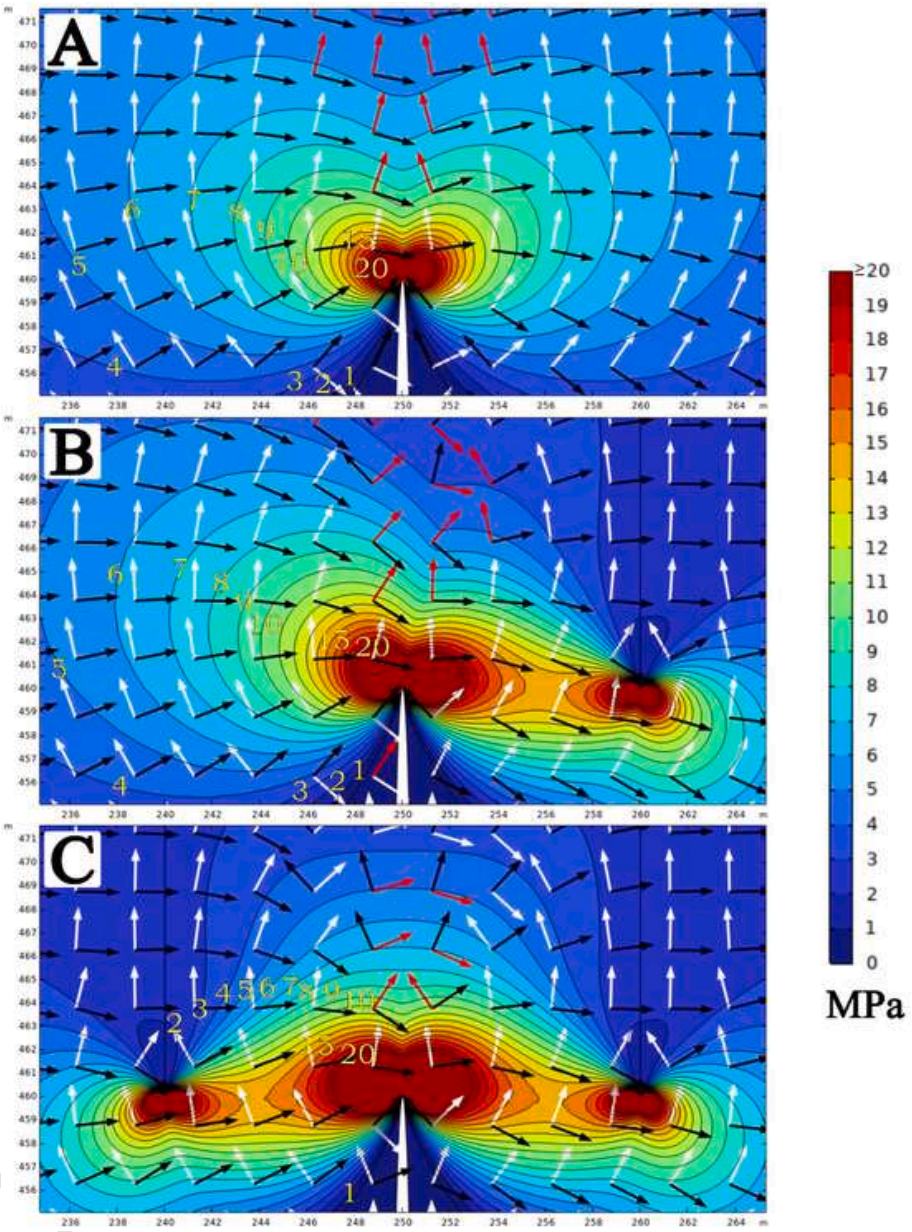

Fig. 8. *(A) Enlargement of the model with no pre-existing fractures (7F). (B) Enlargement of the model with only one pre-existing fracture to the right side of the dike (7D). (C) Enlargement of the model with two pre-existing fractures at the sides of the dike (11U). In all cases, the horizontal distance dike/fracture is 10 m and the dike's tip and fracture's depth is located at 40 m. White arrows σ_1, black arrows σ_3, red arrows σ_2.* (For interpretation of the references to color in this figure legend, the reader is referred to the Web version of this article.)

tween fractures is systematically varied. From left to right, the vertical separation between the dike tip and the fracture base is from 30 m to 0 m. Fracture spacing increases from top to bottom, from 20 m to 100 m. The models in the first line (A, G, N, T) are without pre-existing fractures for comparison. To construct these models, we progressively deepened the vertical fractures, i.e. effectively reducing the vertical separation between the fracture base and the dike tip. This configuration was essential to maintain a constant dike-tip depth (40 m), thereby avoiding stress variations related to proximity to the free surface (Fig. S2). By contrast, deepening the dike-tip while keeping fracture bases fixed would have altered the overall stress field, rendering comparisons across scenarios less meaningful.

The results show that the general stress pattern varies with the pre-existing fractures, the classical "butterfly wings" shape remains but the wings enlarge and are captured by the lower parts of the fractures. A stress shadow appears at the external sides of the fractures, and stress concentration develops at the dike tip and at the base of the fractures. The measured magnitude of tensile stress above the dike tip is highly

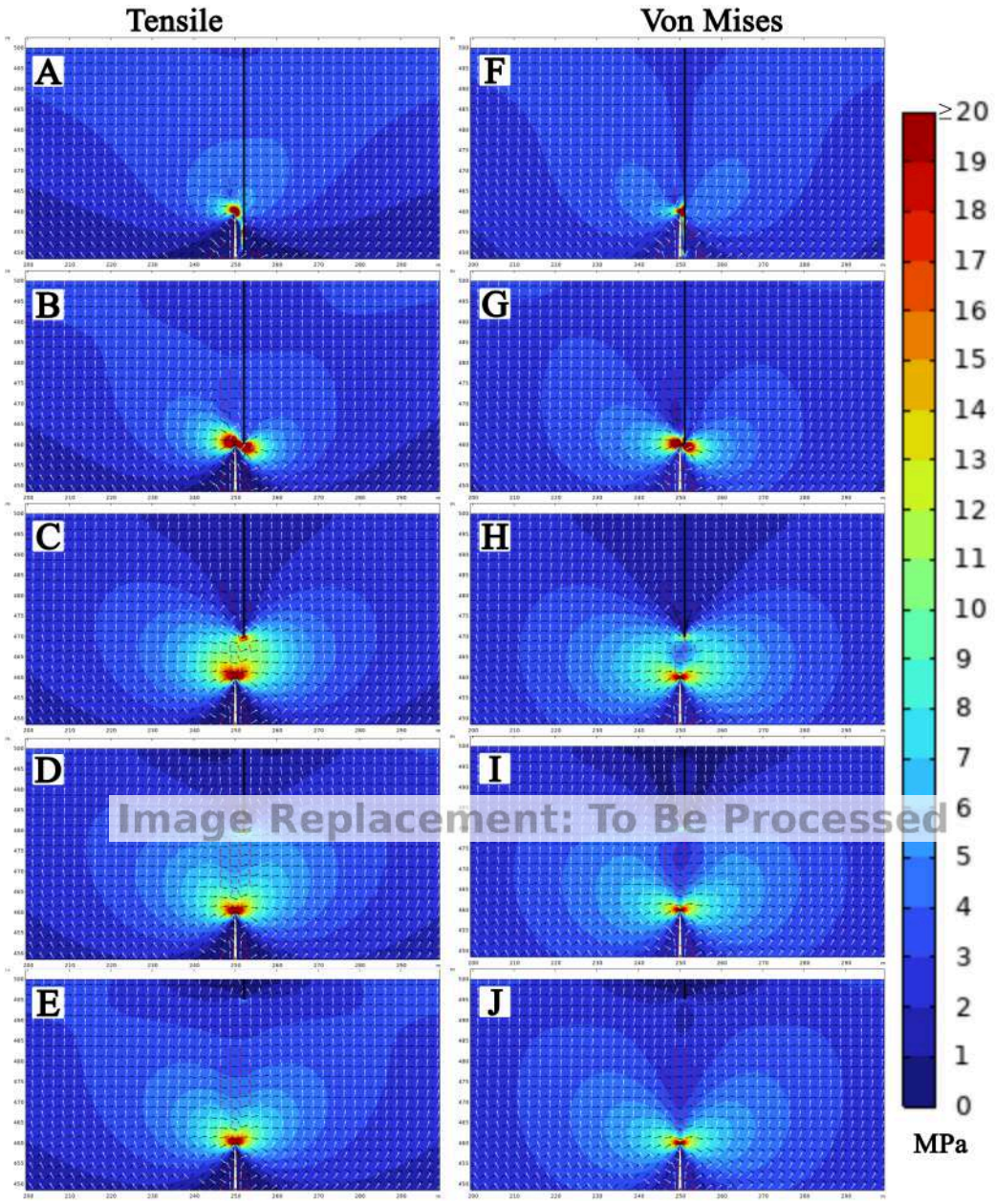
Tensile
Von Mises
A
B
C
D
E
F
G
H
I
J
≥20
19
18
17
16
15
14
13
12
11
10
9
8
7
6
5
4
3
2
1
0
MPa
Image Replacement: To Be Processed

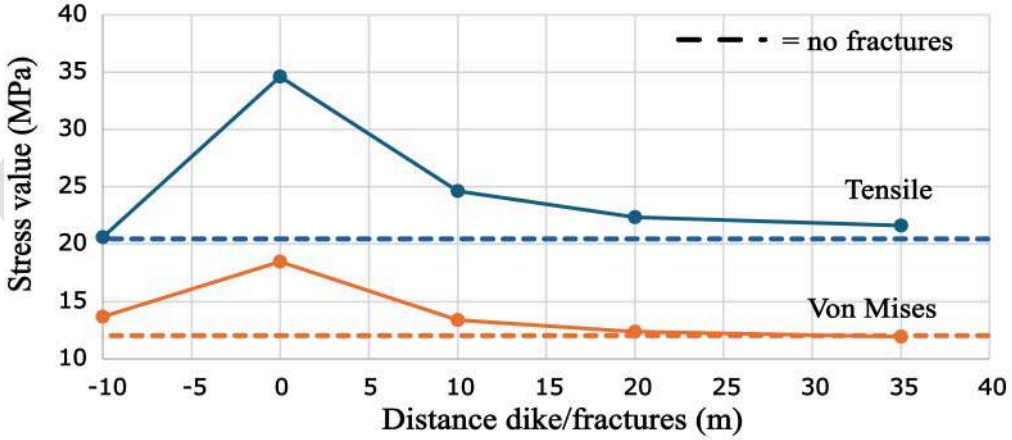
= no fractures
Tensile
Von Mises
Stress value (MPa)
40
35
30
25
20
15
10
-10
-5
0
5
10
15
20
25
30
35
40
Distance dike/fractures (m)

Fig. 9. Effects of the vertical separation between the dike and the fracture base (lower tip) on the tensile and von Mises stress fields near a single pre-existing fracture. From A to E, and from F to J, the dike tip is from 10 m above the fracture base to 35 m below it. The horizontal distance between the dike and the fracture is 2 m for the tensile stress and 1 m for the von Mises stress. White arrows σ_1, black arrows σ_3, red arrows σ_2. Dike overpressure 2 MPa. The dike tip depth is maintained at 40 m. The graph shows the stress value (Y-axis) measured at the dike tip in the case of no pre-existing fractures (dashed line) or with a pre-existing fracture at various vertical distances from the dike. (For interpretation of the references to color in this figure legend, the reader is referred to the Web version of this article.)

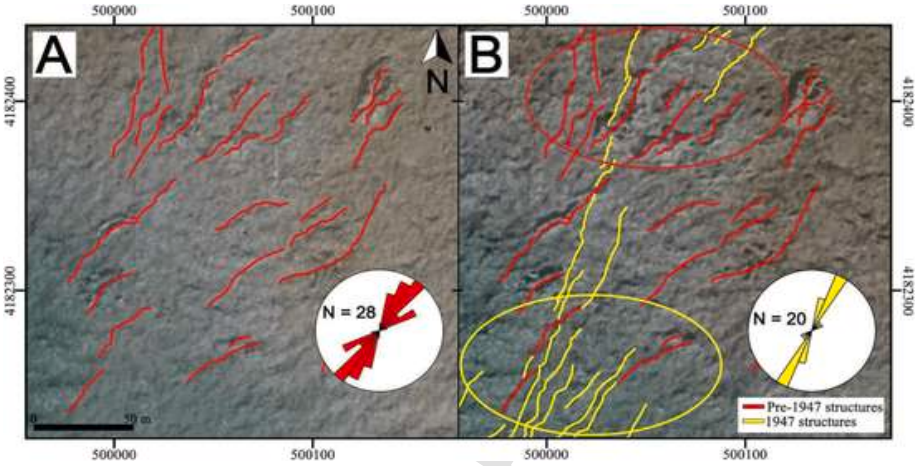

Fig. 10. (A) In the bottom part of this area (1932 orthomosaic), there were a few pre-1947 fractures and in the top part of the same figure there was a higher number of pre-existing fractures. In (B), during the 1947 eruption, several new fractures formed in the lower part of the area and a few new fractures formed on the northern part. Rose diagrams of the respective fractures are shown. Location in Fig. 2.

sensitive to both the vertical offset between the dike and the fracture base, and the horizontal spacing of the fractures. The graph in the lower part of Figure 11 shows that stress at the dike tip increases in the presence of pre-existing fractures. The stress starts to increase when the vertical separation dike/fracture is about 30 m (Line A-F in the graph) for this dike overpressure, and the maximum stress amplification occurs when the dike tip lies just below the fracture base, particularly at moderate fracture spacings (e.g. 20–30 m). The stress increase tends to disappear at fracture separation >140–160 m, which is to say at a distance of the dike from the fracture >70–80 m. The orientation of σ_1 remains vertical and σ_3 horizontal in all models.

The models in Fig. 12 examine scenarios in which the base of the vertical fractures lies progressively deeper than the dike tip, effectively embedding the dike within the fractured domain. In these cases, the classical butterfly wings shape without fractures (for comparison portrayed in models A, G, N, T) is much deformed; stresses tend to concentrate at the base of the fractures and at the dike tip. The presence of the fractures creates an obstacle to the outward propagation of the stresses, i.e. the stresses tend to concentrate in the rock volume in between the fractures.

The graph in the bottom part of Fig. 12 confirms that stress at the dike tip increases in the presence of pre-existing fractures. The stress increase, maximum when the dike tip is at the base of the fractures, becomes gradually lower as the dike tip becomes shallower (the dike propagates to shallower depths) with respect to the fracture base, but remains significantly higher than without fractures. The stress increase tends to become smaller only at larger horizontal separations dike/fractures with respect to the previous models of Fig. 11. Remarkably, the models reveal that even when the fracture base is located tens of meters below the dike tip, the stress field above the dike tip remains influenced by their presence. The orientation of σ_1 remains vertical and σ_3 horizontal in all models.

Figure 13 provides an insight into the mechanical role of an increasing number of pre-existing vertical fractures adjacent to a propagating dike. These models progressively increase the number of fractures (from 0 to 8) and the width of the fracture swarm (20–80 m), and consider, for comparison, a dike tip at the same depth above the fracture base. As in the previous models, the dike overpressure is 2 MPa. For reference, Fig. 13A and F shows the same setting but without any fracture. The results show a clear change in the general stress pattern in the case of presence of pre-existing fractures. Already with two fractures (Fig. 13B), the tensile stress becomes concentrated in the rock volume between them, with a larger zone of stress concentration above the dike tip. Other zones of higher stress concentration coincide with the base of the fractures. At the surface, the tensile stress magnitude decreases when pre-existing fractures are present, and further decreases with an increasing number of fractures. With an increasing number of fractures (Fig. 13C, D, E), the higher tensile stress remains concentrated above the dike tip and confined by the inner fractures. Other zones of stress concentration coincide with all the fracture bases, with decreasing width of these zones outward. In regard to the orientation of the stresses, σ_1 varies from being vertical to sub-vertical above the dike tip, and the σ_3 is from horizontal to sub-horizontal. In the area of higher tensile stress above the dike tip, the sub-vertical σ_1 dips outward with respect to the dike. Along the central and upper parts of the fractures, the σ_3 is perpendicular to the fractures and the σ_1 is parallel to them. Along the lower part of the fractures, the σ_3 is parallel to the fractures and the σ_1 is normal to them.

Regarding the von Mises stress, with two fractures (Fig. 13G) it becomes concentrated in the rock volume between the fractures, with a larger zone of stress concentration above the dike tip. Differently from the tensile stress, the von Mises stress concentration is around most of the length of the fractures. Other zones of higher stress concentration coincide with the base of the fractures. At the surface, the stress magnitude decreases in case of presence of pre-existing fractures, and further decreases with an increasing number of fractures. With an increasing number of fractures (Fig. 13H, I, J), the higher von Mises stress remains confined by the inner fractures, and the stress shadow in the rock volume outside the fracture swarm increases. Other zones of stress concentration coincide with all the fracture bases, with decreasing width of these zones outward. In regards to the orientation of the stresses in the zones of maximum concentration of the von Mises stress, along the cen-

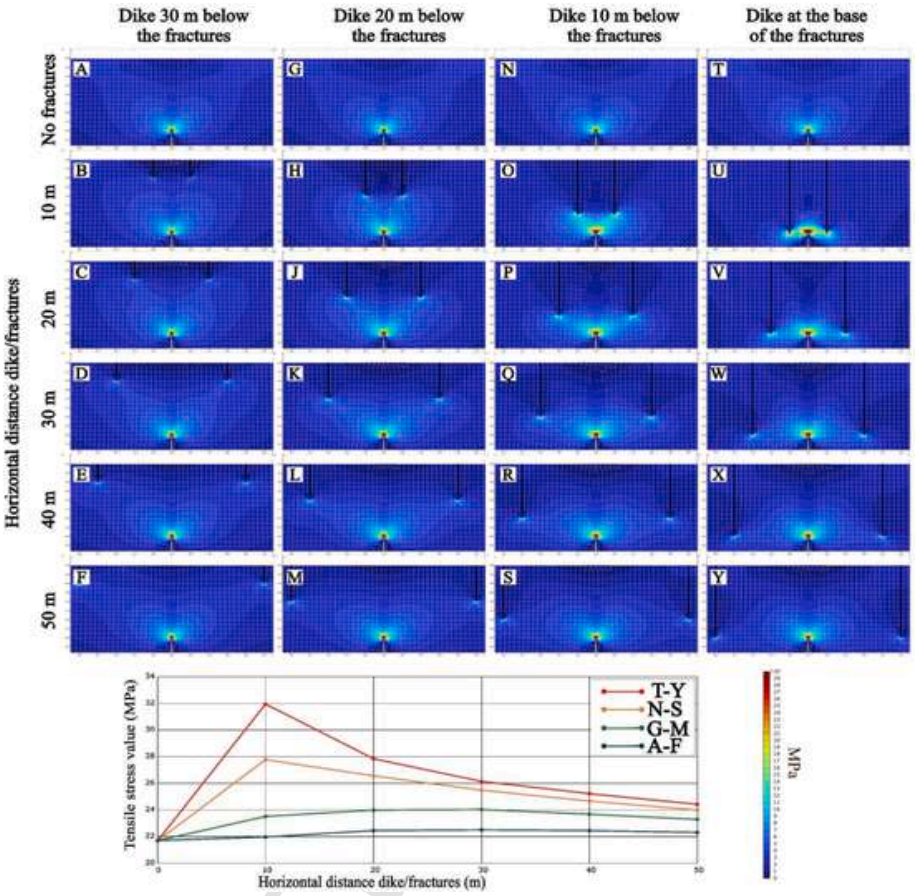

Fig. 11. Effects of vertical separation dike/fracture and spacing between fractures on the tensile stress field above a pressurized dike. Each column shows models with a fixed fracture spacing and varying depth of the fracture base relative to the dike tip: from 30 m (left) to 0 m (right, i.e., fracture base coincides with the dike tip). The dike tip remains fixed at a depth of 40 m. Fracture spacing increases from top to bottom. Fractures have an aperture (opening) of 1 cm. Dike overpressure is set to 2 MPa. Dike dimensions are 150 m in length and 2 m in thickness. Young's modulus of the host rock is 11 GPa, while that of the fractures is 0.001 GPa. The graph in the bottom shows the mean tensile stress as a function of dike-fracture vertical separation for different fracture spacings.

tral-upper parts of the fractures, the σ_3 is perpendicular to the fracture plane and the σ_1 is parallel to it. Along the lower part of the fractures, the σ_3 is parallel and the σ_1 is normal to the fracture plane.

5. Discussion

5.1. General versus local volcanotectonic pattern

Comparison of the general pattern of the 1947 fracture swarm with the previously existing fracture system in the same area (Fig. 2), suggests the presence of an inherited general weakness zone, which belongs to the North-East Rift of Mt. Etna. This rift is subject to a tensional stress oriented from WNW-ESE to NW-SE (Tibaldi et al., 2021). Although it is out of the scope of this work to deeply discuss the origin of the stress field here, we suggest that in the shallower part of the Etna cone, the local stress field could be mainly linked to the gravitational instability of the volcano eastern flank (Borgia et al., 1992; Rust and Neri, 1996; Tibaldi and Groppelli, 2002). Anyway, a contribution from regional tectonic extensional stresses cannot be ruled out (Monaco et al., 1997, 2005; Giacomoni et al., 2012), and this might be more important in the deeper parts of the volcano and of course in the substratum. Moreover, the rift separates the relatively stable northwestern Mt. Etna flank from the unstable eastern flank, thus acting as a major boundary in the upper cone. Also, this rift concentrated most of the intrusive activity in the last centuries, with several dikes that upraised here vertically or propagated laterally from the summit vent zone (Monaco et al., 2005; Aloisi et al., 2006; Tibaldi et al., 2025). The possible propagation of the 1947 dike along a previous dike path is thus consistent with the aforementioned characteristics of the North-East Rift. This observation aligns with the previous literature emphasizing the role of the high fracture density, among which the Etna's North-East Rift represent a prominent example (Mazzarini and Armienti, 2001). It is also coherent with previous works conducted elsewhere that have recognized, in the field, multiple intrusions in the field along the same dike path (e.g. Paquet et al., 2007; Glazner et al., 2008). In regard to the possibility that a topographic relief might attract dikes, this was demonstrated for large topographic highs (Muller et al., 2001), whereas more investigations are necessary in the case of more limited reliefs such as the North-East rift.

On a closer look, our geological observations on the key site of Fig. 6 demonstrate that a large number of the 1947 eruptive vents originated nearby pre-existing fractures, but only in one case a vent coincides with a previous fracture. Moreover, there is a difference of 10° between the pre-1947 fracture alignment and the 1947 vent alignment. This difference can be appreciated also by all the other morphometric parameters that indicate the orientation of the magma-feeding fracture below a pyroclastic cone (Tibaldi, 1995), including the elongation of the cone base and crater, the orientation of the depressed points of the crater rim, and the breaching trend. Also in the other studied key site of Fig. 10, there is a misalignment between the pre- and syn-1947 fractures. Moreover, at several sites along the 1947 fracture swarm, we noticed a variation in number of the syn-1947 fractures that is inversely proportional to the number of pre-existing discontinuities.

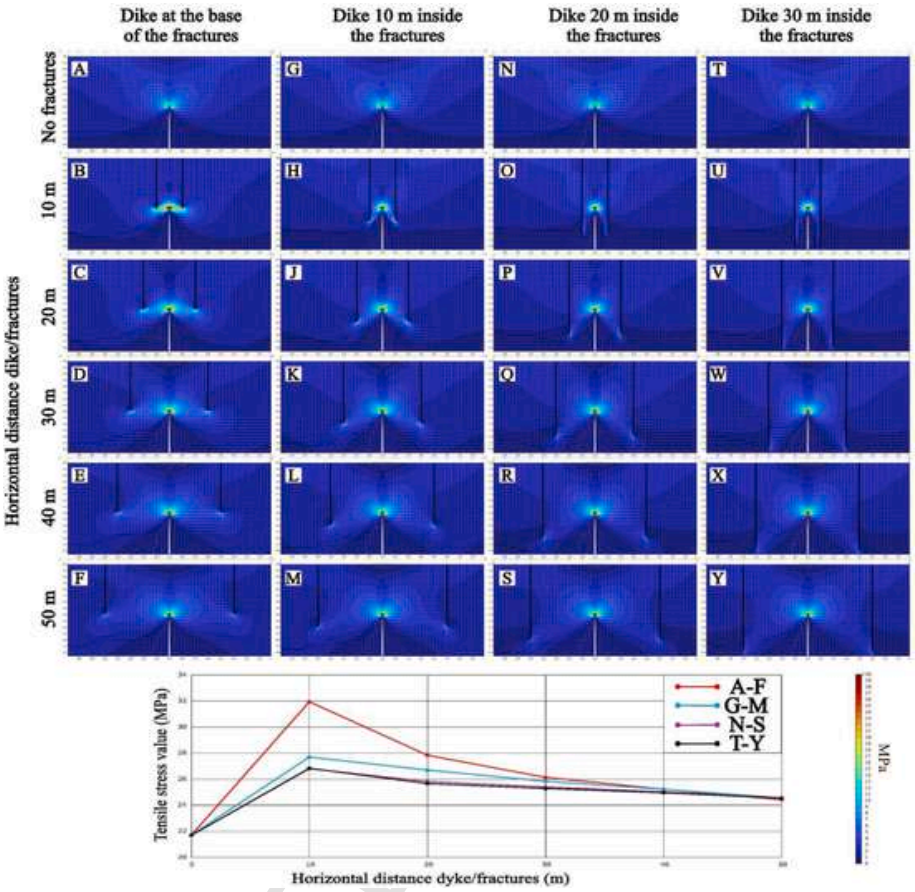

Fig. 12. Effects of vertical fracture depth on the stress field above a dike. In this series of models, the dike tip is fixed at a depth of 40 m, while the base of the vertical fractures lies progressively deeper, from coinciding with the dike tip (left) to 30 m below (right). Fracture openings are 1 cm. dike overpressure is 2 MPa; dike length is 150 m, and width is 2 m. The Young's modulus of the host rock is 11 GPa, and that of the fractures is 0.001 GPa. The graph (bottom) shows the mean tensile stress as a function of dike-fracture vertical separation for different fracture spacings.

In conclusion, based on the field data, we suggest that the 1947 dike followed, in general, a path that coincided with a previous intrusion due to the general predisposing settings, thereby possibly forming a multiple dike as is very common (Gudmundsson, 2025). But locally, the 1947 dike also diverted from the previous path, highlighting the complex three-dimensional mechanical interplay between dike geometry, vent location, opening of new fractures, and pre-existing fracture architecture. The numerical models that we developed, help to better understand, at a detailed scale, how inherited discontinuities can interact with magma propagation.

5.2. *Single pre-existing fracture*

The models with one fracture show that, in the case a rising dike meets directly a pre-existing fracture (Fig. 7A), the higher tensile stress propagates around the base of the fracture, with a vertical σ_1 and a horizontal σ_3. These can be logically interpreted as positive conditions for opening the fracture and dike intrusion within it. The tensile stress also propagates upward, at the sides of the fracture, depicting butterfly wings very similar to the case without a pre-existing fracture. In most of the paper we give just indications of relative variations of the stress amount in the host rock depending on the various variables, remaining on qualitative evaluation. We give here just one possible quantitative example considering the investigated conditions of Fig. 7A: with a dike tip at a depth of 30 m, the tensile stress field in the range of 3–4 MPa intercepts the surface suggesting possible fissure opening at the sides of the dike. This is based on the fact that fracturing is expected if the tensile stress is at least equal to the in-situ tensile strength (Gudmundsson, 2011). In laboratory experiments, tensile strengths of 5 MPa were obtained for basalts, using intact samples (Graue et al., 2011; Perras and Diederichs, 2014). The in-situ tensile strengths of rocks obtained by hydraulic fracture experiments have instead most common values of 2–4 MPa (Haimson and Rummel, 1982; Daemen and Schultz, 1995; Amadei and Stephansson, 1997; Gudmundsson, 2011), which have already been used in previous numerical studies (Al Shehri and Gudmundsson, 2018; Bazargan and Gudmundsson, 2019). In the case of diffuse columnar joints and pre-existing fractures of other origin, the rock masses are weakened and even lowest values of in-situ tensile strength may be appropriate for modeling. For a fault to slip, the von Mises shear stress should be at least equal to the shear strength, which is normally about double the tensile strength (Haimson and Rummel, 1982; Schultz, 1995; Gudmundsson, 2011). For the von Mises stress thus, the values at the surface that we found are generally lower than the expected value for faulting.

For all the remaining interpretations, we focus our attention on the areas of main variations of tensile and von Mises stresses. The models with an upward-propagating dike that is not aligned with the pre-existing single fracture show interactions with the base of the fracture, with a horizontal enlargement of the zone of highest tensile stress that connects the dike tip to the fracture base. In this zone, the stress reorientation suggests a possible nucleation of a new fracture curving toward the pre-existing one, in which case the propagating dike could become deflected into the pre-existing vertical fracture. The asymmetric perturbation observed in Fig. 7 (or the zoom in Fig. 8B), closely resem-

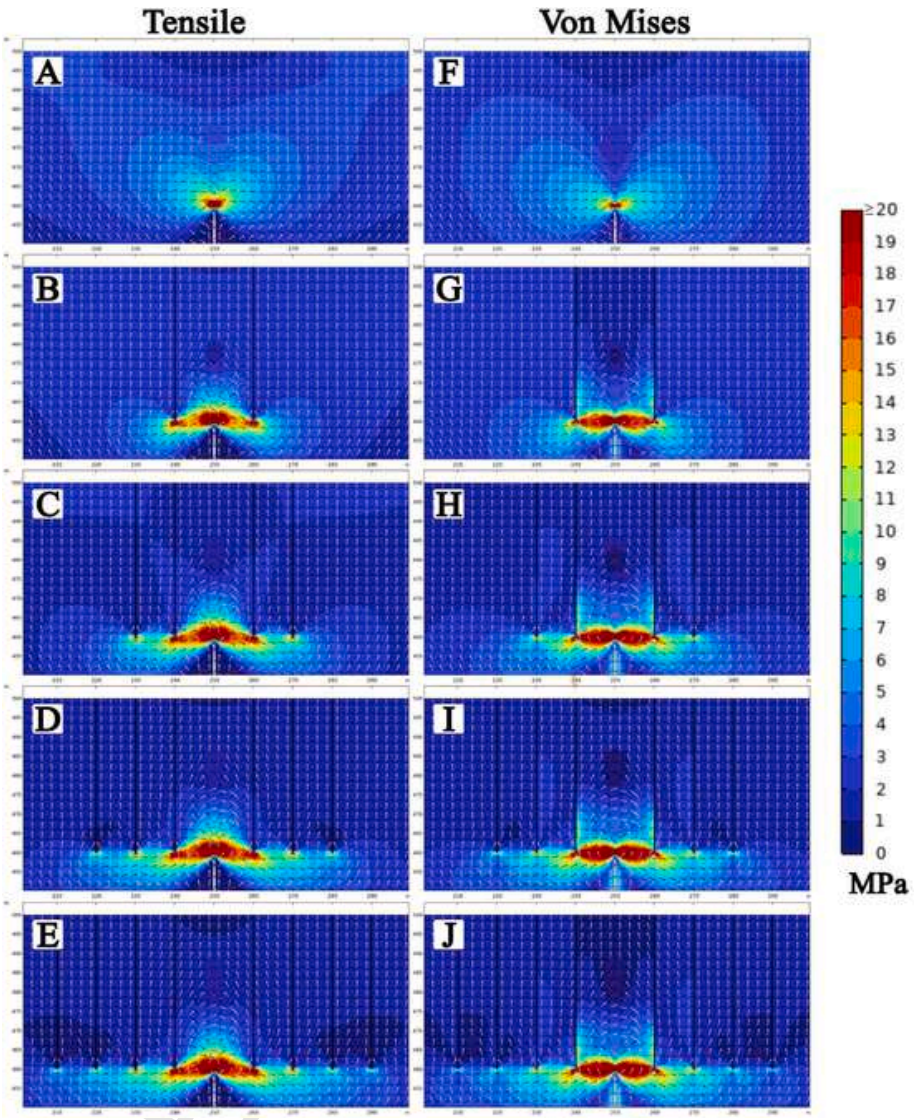

Fig. 13. Different numbers of pre-existing vertical fractures parallel with a dike. A and F are without pre-existing vertical fractures. Models B-G, C-H, D-I and E-J are respectively with 2, 4, 6, and 8 vertical fractures 10, 20, 30 and 40 m from the central dike. The down-dip length (dip-dimension) of all fractures is 40 m. Dike tip is at the depth of 40 m. Fracture openings are 1 cm. Dike overpressure = 2 MPa. Dike length (dip-dimension) = 150 m and thickness (opening) = 2 m. E Host rock = 11 GPa. E Fractures = 0.001 GPa.

bles the mechanical behavior described in studies of overlapping/underlapping fractures under tension (Lamarche et al., 2018). Specifically, the curvature observed between the propagating dike and the pre-existing vertical fracture is analogous to the development of hook-shaped fractures that emerge between slightly overlapping or underlapping fractures (Lamarche et al., 2018). This structural pattern is also characteristic of overlapping spreading centres on the ocean floor, where similar stress configurations govern the geometry of fracture propagation (Francheteau et al., 1992; Lister and Kerr, 1991). Such patterns have been rigorously explored in analytical fracture mechanics, highlighting the role of local stress concentration and interaction effects in guiding fracture paths. Our models capture this curvature effectively, reinforcing the idea that even a single structural discontinuity can trigger complex dike-fracture interactions consistent with fracture mechanics theory. It should be noted, however, that such a deflection of a dike to the existing vertical tension fracture depends primarily on energy considerations in that the dike tends to follow the path of least action or, when the velocity is slow, the path of minimum potential energy (Gudmundsson, 2022). If σ_3 is horizontal, as it commonly is close to the surface in a rifting environment, and if the tensile strength across the existing tension fracture is similar to that across existing cooling joints in the rocks above the tip of the propagating dike, then the dike would be more likely to continue along its vertical path toward the surface rather than become deflected into the existing tension fracture.

In the three zoomed models (Fig. 8) all the parameters are equal apart from the absence of fractures, or the presence of one fracture or two fractures. In both the latter cases, the distance between the dike and the fracture is 10 m. In the two models with fractures (Fig. 8B, C), σ_1 is rotated suggesting possible propagation of a new fracture from the dike tip towards the pre-existing fracture. At a larger distance above the dike tip (about 4 m in these models), the new fracture in front of the dike tip can further propagate along the same plane containing σ_1 and σ_2, although σ_1 interchanges with σ_2. Instead, in the case with two (or more) pre-existing fractures, all the stresses rotate and about 4 m above the dike tip, σ_3 assumes a subvertical attitude, suggesting a shorter upward fracture propagation. In a time perspective, this means that with a single pre-existing fracture at the side of a dike, dike-tip propagation to-

ward the pre-existing fracture, if it happens, would be faster than in the case of two or more pre-existing fractures.

Apart from this possibility of linking between the dike and a single pre-existing fracture, we also highlight the fact that the tensile stress concentration is greatest above the dike tip, and there σ_1 is vertical and σ_3 is horizontal. This means that the dike also has the possibility of propagating upward maintaining a vertical attitude – as was discussed above (cf. Gudmundsson, 2022). The vertical propagation of the dike tip is, however, also facilitated by the presence of a close pre-existing fracture, as witnessed by the values of tensile stress that are larger at the dike tip in this case with respect to the case of an unfractured host rock. The probability of upward dike propagation instead of bending towards the pre-existing fracture, increases with the distance dike/fracture. At the explored conditions, at distances dike/fracture larger than 10–20 m, the models indicate this higher probability, which is consistent with the field data collected at Mt. Etna, where the 1947 vents are located up to 11 m from the nearest pre-existing fracture. We are aware that a fracture trace at the surface can slightly differ from the deeper part; in volcanic terrains this might be due, for example, to the presence at the surface of "aa" lava flows. These flows have a blocky surface that may conceal the real deeper fracture trace. Anyway, in our studied area, most of the 1947 dyke developed over the 1614–1624 pahoehoe lava field, which, according to Guest et al. (1984), may have an average vertical thickness of ~100 m. Moreover, our observations and numerical models focus only on the shallower part of the succession. We thus retain that the location of the fractures at the surface cannot differ sensibly from their counterpart at a depth of a few tens of meters.

Regarding the von Mises stress, although there is a concentration of higher values along the lower part of the pre-existing fracture, since σ_1 here is vertical and σ_3 is horizontal, it is not expected to develop faulting along them. It can instead occur that when the dike tip moves to shallower settings, the pre-existing fracture can be reactivated as a fissure.

The presence of pre-existing open fissures instead of narrow fractures does not change the observed general patterns. Changes in dike overpressure also do not modify the aforementioned observations, apart from increasing the absolute stress values.

5.3. Multiple pre-existing fractures

Concerning the effects of multiple pre-existing fractures on a dike propagation, the results show that the introduction of additional fractures enhances tensile stress above the dike tip. This, combined with the systematic vertical σ_1 and horizontal σ_3 near the dike tip, means that there is a higher probability of upward propagation of the fracture in front of the dike tip, followed by further dike propagation if the magma overpressure is enough. At further distance above the dike tip, but again in the area of higher tensile stress, the sub-vertical attitude of the σ_1 that dips outward with respect to the dike, indicates a very low probability of propagation of the dike towards the near fractures.

At the explored conditions, the stress increase at the dike tip starts when the difference of depth between it and the base of the pre-existing fractures is in the order of 30 m for an overpressure of 2 MPa. The stress increase is also sensitive to the horizontal spacing of fractures: our models suggest that the maximum stress increase is reached when the dike tip is at the base of the pre-existing fractures, with a spacing of the fractures of about 20 m. When the dike tip is deeper, the stress increase is lower and reaches the maximum values when the distance between the fractures is in the order of 40–60 m. This effect disappears if the already existing fractures are located at distances of 60–100 m from the dike and depending on the dike depth. In conclusion, the suitable orientation of the principal stresses and the increase in magnitude of the tensile stress at the dike tip, suggest that a dike uprising nearby, or in the middle, of already existing fractures receive a sort of “booster” enhancing its probability of further propagation.

As for the more general stress field in the surrounding of a propagating dike, our results indicate that pre-existing fractures at the dike side creates stress shadows on the outward sides. This can be explained in mechanical terms, by the role exerted by a discontinuity in the rock mass. Over the past decades, much research based on numerical models has been carried out regarding the factors that can affect dike propagation, within which the stress field is fundamental (e.g., Gudmundsson, 2003; Maccaferri et al., 2010, 2011, 2016; Geshi et al., 2012; Philipp et al., 2013; Barnett and Gudmundsson, 2014; Rivalta et al., 2015; Drymoni et al., 2020, 2023). Dike arrest can occur because of stress barriers, namely layers or units where the local stress field is unfavorable to dike propagation (Gretener, 1969; Gudmundsson, 2011). Other processes that suppress stress transmission are Cook-Gordon delamination and elastic mismatch, where there is a strong contrast in Young's modulus across a contact (Gudmundsson, 2011). Pre-existing fractures represent a feature with very low mechanical characteristics, which inhibit further transmission of most of the stress field across the discontinuity. The result is that most stresses are confined in the rock mass bounded by the fractures. This may explain why we can have that sort of “booster” enhancing possible dike propagation.

The concentration of stress at the dike tip and around the bases of pre-existing vertical fractures are reflected at the surface by a decrease of tensile stress transmission with respect to an unfractured overburden. This means that there is a lower probability of formation of new fractures if pre-existing fractures are already widespread. This observation is consistent with our field data at Mt. Etna (Fig. 10), where we observed that new fractures, during the 1947 event, developed where there were a few pre-existing fractures, and where there were several pre-existing fractures, a few, or not at all, new fractures developed. Similarly, our models also indicate a decrease of the von Mises stress near the surface in the case of pre-existing fractures, and this decrease is larger with increasing number of pre-existing discontinuities. This means that when a dike is approaching the surface across a rock volume with already well-developed vertical fractures, there is a lower probability of development of new faults, or shear remobilization of already existing discontinuities, at the surface.

We are aware that this study simplifies the natural conditions, such as the presence of horizontal discontinuities or intra-layer features within the lava flows succession beneath the surface, as well as the influence of slope angle, which undoubtedly plays a key role. Nevertheless, our aim was to investigate the effects that different numbers and configurations of pre-existing structures have on a dike approaching the surface. Our numerical modelling results, consistent with the field observations already published by Tibaldi et al. (2025) along the 1947 fracture system, suggest that such structures exert a strong influence on dike propagation, either inhibiting their ascent or facilitating the arrival at the surface, potentially leading to eruption.

6. Conclusions

In order to contribute to a better understanding of the conditions and mechanisms under which dikes interact with pre-existing vertical fractures, we analyzed some key examples in the field and then developed a series of FEM numerical models anchored to the geological and structural data. Along the North-East Rift, on the northern flank of Mt. Etna, Italy, we mapped in detail two sections of the fracture swarm and eruptive vents formed during the 1947 eruption, and compared them with the pre-existing fracture field. Our data complete more extensive field data published in Tibaldi et al. (2025). Here below the main results:

- Field data show that the 1947 dike followed, in general, the path of a previous dike. At a more local, detailed scale, the locations of the 1947 eruptive vents are shifted up to 11 m laterally with respect to single pre-1947 fractures.

- The numerical models with a single pre-existing fracture, show an interaction with the base of the fracture, with a horizontal enlargement of the zone of highest tensile stress that connects the dike tip to the fracture base. In this zone, the stress reorientation suggests a possible scenario given by the nucleation of a new fracture bending toward the pre-existing one, possibly followed by the deflection of the propagating dike that reaches the pre-existing vertical fracture. Such a propagation path, however, would form only if it coincided with the path of least action or minimum potential energy.
- By contrast, the high value of tensile stress concentrate above the dike tip, and the local orientation of σ_1 and σ_3, suggest that the dike may simply continue along is vertical path, using existing joints in the lava pile and maintaining its orientation as to being perpendicular to the minimum compressive (maximum tensile) principal stress, σ_3. But in both cases (curved or vertical close-to-surface path), the dike propagation is facilitated by the presence of a close pre-existing tension fractures, as demonstrated by the values of tensile stress that are larger at the dike tip with respect to the case of an unfractured host rock.
- Field data in another key site of the 1947 eruption, indicate that in areas where few fractures were already present, a significant number of new fractures developed during the successive 1947 event. Conversely, where the density of pre-existing fractures was already high, few new fractures formed.
- Numerical models varying the number of pre-existing fractures, their distance from an upward-propagating dike, and the depth difference between the dike tip and the fracture base, show that the introduction of additional fractures enhances tensile stress above the dike tip. This, combined with the systematic vertical σ_1 and horizontal σ_3 near the dike tip, means that there is a higher probability of upward propagation of the dike.
- For the explored conditions, the stress increase above the dike tip is also sensitive to the horizontal spacing of fractures. This is reached when the dike tip is at the base of the pre-existing fractures, with a spacing of the fractures of about 20 m.
- This concentration of stress around the dike tip is compensated by a decrease of tensile stress at the surface, which means a lower probability of formation of new fractures if pre-existing fractures are already widespread. Similarly, the von Mises stress tends to decrease near the surface in the case of pre-existing fractures. This suggests that pre-existing fractures act also as shear stress sinks, reducing the likelihood of new fault formation in the shallow rocks above the dike. The evolution of both tensile and von Mises stress fields underscores the dual role of fracture networks in both facilitating and modulating dike-induced deformation, consistent with the field data of the 1947 diking event.
- The present field and numerical results highlight the complex mechanical interplay between dike geometry and pre-existing fracture architecture. They emphasize that not only the proximity but also the relative positioning of fractures and propagating dikes in the vertical dimension can significantly alter the local stress regime and potentially influence dike-propagation paths and, therefore, the eventual location of dike-fed volcanic fissures. An upward-propagating dike located nearby, or in the middle of, already existing vertical fractures, receives a sort of “booster” enhancing its probability of further propagation.

Our integrated analysis, combining detailed mapping of the 1947 eruption fractures with FEM models constrained by geological data, provides robust insights into these interactions, with direct implications for volcanic hazard assessment. Fracture density and spacing can either enchant or inhibit upward dike propagation, controlling the likelihood of fracture development and consequent magma infilling and its propagation. These findings highlight the importance of incorporating structural heterogeneities into predictive models of magma transport, improving the identification of areas at higher risk for dike-fed eruptions.

CRediT authorship contribution statement

A. Luppino: Writing – review & editing, Writing – original draft, Visualization, Software, Methodology, Investigation, Formal analysis, Data curation. **F.L. Bonali:** Writing – review & editing, Methodology, Investigation, Conceptualization. **A. Gudmundsson:** Writing – review & editing, Data curation, Conceptualization. **A. Tibaldi:** Writing – review & editing, Writing – original draft, Supervision, Investigation, Funding acquisition, Conceptualization.

Declaration of competing interest

The authors declare the following financial interests/personal relationships which may be considered as potential competing interests: Alessandro Tibaldi reports travel was provided by International Lithosphere Program ILP. If there are other authors, they declare that they have no known competing financial interests or personal relationships that could have appeared to influence the work reported in this paper.

Acknowledgements

We acknowledge the very useful suggestions of the reviewers Francesco Mazzarini and Carmelo Monaco on a previous version of the manuscript. This work has been carried out under the aegis of Task Force II of the International Lithosphere Program (Leader A. Tibaldi). This manuscript is also an outcome of the Virtual Reality lab for Earth Sciences - GeoVires (https://geovires.unimib.it/), University of Milano-Bicocca. Agisoft Metashape is acknowledged for photogrammetry processing. The work was also supported by funding of the Doctoral school of the University of Milan-Bicocca. Sincerely thanks to Emanuela De Beni and Massimo Cantarero for granting the use of drone photos and for the support during the field surveys.

Data availability

Data will be made available on request.

Appendix A. Supplementary data

Supplementary data to this article can be found online at https://doi.org/10.1016/j.jsg.2025.105563.

References

Al Shehri, A., Gudmundsson, A., 2018. Modelling of surface stresses and fracturing during dyke emplacement: application to the 2009 episode at Harrat Lunayyir, Saudi Arabia. J. Volcanol. Geoth. Res. 356, 278–303.
Aloisi, M., Bonaccorso, A., Gambino, S., 2006. Imaging composite dike propagation (Etna, 2002 case). J. Geophys. Res. Solid Earth 111 (B6).
Amadei, B., Stephansson, O., 1997. Rock Stress and its Measurement. Springer Science & Business Media.
Anderson, E.M., 1951. The Dynamics of Faulting and Dyke Formation with Applications to Britain, second ed. Oliver and Boyd, Edinburgh, UK.
Antoniou, V., Bonali, F.L., Nomikou, P., Tibaldi, A., Melissinos, P., Mariotto, F.P., et al., 2020. Integrating virtual reality and GIS tools for geological mapping, data collection and analysis: an example from the Metaxa Mine, Santorini (Greece). Appl. Sci. 10 (23), 8317.
Azzaro, R., Branca, S., Gwinner, K., Coltelli, M., 2012. The volcano-tectonic map of Etna volcano, 1: 100.000 scale: an integrated approach based on a morphotectonic analysis from high-resolution DEM constrained by geologic, active faulting and seismotectonic data. Ital. J. Geosci. 131 (1), 153–170.
Baer, G., Beyth, M., Reches, Z., 1994. Dikes emplaced into fractured basement, Timna Igneous Complex, Israel. J. Geophys. Res. 99, 24039–24050.
Barnett, Z.A., Gudmundsson, A., 2014. Numerical modelling of dykes deflected into sills to form a magma chamber. J. Volcanol. Geoth. Res. 281, 1–11.
Bazargan, M., Gudmundsson, A., 2019. Dike-induced stresses and displacements in layered volcanic zones. J. Volcanol. Geoth. Res. 384, 189–205.

Bonali, F.L., Corazzato, C., Tibaldi, A., 2012. Elastic stress interaction between faulting and volcanism in the Olacapato–San Antonio de Los Cobres area (Puna plateau, Argentina). Global Planet. Change 90, 104–120.
Bonali, F.L., Corti, N., Mariotto, F.P., De Beni, E., Bressan, S., Cantarero, M., et al., 2024a. 3D study of dyke-induced asymmetric graben: the 1971 Mt. Etna (Italy) case by structural data and numerical modelling. J. Struct. Geol. 187, 105231.
Bonali, F.L., Vitello, F., Kearl, M., Tibaldi, A., Whitworth, M., Antoniou, V., et al., 2024b. GeaVR: an open-source tools package for geological-structural exploration and data collection using immersive virtual reality. Applied Computing and Geosciences 21, 100156.
Borgia, A., Ferrari, L., Pasquarè, G., 1992. Importance of gravitational spreading in the tectonic and volcanic evolution of Mount Etna. Nature 357 (6375), 231–235.
Branca, S., Coltelli, M., Groppelli, G., Lentini, F., 2011. Geological map of Etna volcano, 1: 50,000 scale. Italian Journal of Geosciences 130 (3), 265–291.
Branca, S., Del Carlo, P., 2005. Types of eruptions of Etna volcano AD 1670–2003: implications for short-term eruptive behaviour. Bull. Volcanol. 67, 732–742.
Browning, J., Gudmundsson, A., 2015. Caldera faults capture and deflect inclined sheets: an alternative mechanism of ring dike formation. Bull. Volcanol. 77, 1–13. https://doi.org/10.1007/s00445-014-0889-4.
Browning, J., Karaoğlu, Ö.Z.G.Ü.R., Bayer, Ö., Turgay, M.B., Acocella, V., 2021. Stress fields around magma chambers influenced by elastic thermo-mechanical deformation: implications for forecasting chamber failure. Bull. Volcanol. 83 (7), 48.
Corti, N., 2024. Analysis of Deformation and Stress Regimes Associated with Dike Emplacement. University of Milan-Bicocca. Doctoral dissertation.
Corti, N., Bonali, F.L., Russo, E., Drymoni, K., Mariotto, F.P., Gudmundsson, A., et al., 2023. Feeders vs arrested dikes: a case study from the Younger Stampar eruption in Iceland. J. Volcanol. Geoth. Res. 443, 107914.
Daemen, J J.K., & Schultz, R A. Proceedings of the 35th U.S. Symposium on Rock Mechanics. Netherlands..
De Guidi, G., Barberi, G., Barreca, G., Bruno, V., Cultrera, F., Grassi, S., et al., 2015. Geological, seismological and geodetic evidence of active thrusting and folding south of Mt. Etna (eastern Sicily): revaluation of "seismic efficiency" of the Sicilian Basal Thrust. J. Geodyn. 90, 32–41.
Delaney, P.T., Pollard, D.D., Ziony, J.I., McKee, E.H., 1986. Field relations between dikes and joints: emplacement processes and paleostress analysis. J. Geophys. Res. Solid Earth 91, 4920–4938. https://doi.org/10.1029/JB091iB05p04920.
Drymoni, K., Browning, J., Gudmundsson, A., 2020. Dyke-arrest scenarios in extensional regimes: insights from field observations and numerical models, Santorini, Greece. J. Volcanol. Geoth. Res. 396, 106854.
Drymoni, K., Browning, J., Gudmundsson, A., 2021. Volcanotectonic interactions between inclined sheets, dykes, and faults at the Santorini Volcano, Greece. J. Volcanol. Geoth. Res. 416, 107294. https://doi.org/10.1016/j.jvolgeores.2021.107294.
Drymoni, K., Russo, E., Tibaldi, A., Corti, N., Bonali, F.L., Mariotto, F.P., 2023. Dyke-induced graben formation in a heterogeneous succession on Mt. Etna: insights from field observations and FEM numerical models. J. Volcanol. Geoth. Res. 433, 107712.
Ferlito, C., Nicotra, E., 2010. The dyke swarm of Mount Calanna (Etna, Italy): an example of the uppermost portion of a volcanic plumbing system. Bull. Volcanol. 72, 1191–1207.
Francheteau, J., Armijo, R., Cheminee, J.L., Hekinian, R., Lonsdale, P., Blum, N., 1992. Dyke complex of the East Pacific Rise exposed in the walls of Hess Deep and the structure of the upper oceanic crust. Earth Planet Sci. Lett. 111 (1), 109–121.
Gaete, A., Kavanagh, J.L., Rivalta, E., Hazim, S.H., Walter, T.R., Dennis, D.J., 2019. The impact of unloading stresses on post-caldera magma intrusions. Earth Planet Sci. Lett. 508, 109–121.
Gambino, S., Barreca, G., Bruno, V., De Guidi, G., Ferlito, C., Gross, F., Mattia, M., Scarfì, L., Monaco, C., 2022. Transtension at the Northern termination of the Alfeo-Etna fault System (Western Ionian Sea, Italy): seismotectonic implications and relation with Mt. Etna volcanism. Geosciences 12 (3), 128.
Garduno, V.H., Neri, M., Pasquarè, G., Borgia, A., Tibaldi, A., 1997. Geology of the NE-Rift of Mount Etna (Sicily, Italy). Acta Vulcanol. 9, 91–100.
Geshi, N., Browning, J., Kusumoto, S., 2020. Magmatic overpressures, volatile exsolution and potential explosivity of fissure eruptions inferred via dike aspect ratios. Sci. Rep. 10 (1), 9406.
Geshi, N., Kusumoto, S., Gudmundsson, A., 2012. Effects of mechanical layering of host rocks on dike growth and arrest. J. Volcanol. Geoth. Res. 223, 74–82.
Geshi, N., Neri, M., 2014. Dynamic feeder dyke systems in basaltic volcanoes: the exceptional example of the 1809 Etna eruption (Italy). Front. Earth Sci. 2, 13.
Giacomoni, P.P., Ferlito, C., Alesci, G., Coltorti, M., Monaco, C., Viccaro, M., Cristofolini, R., 2012. A common feeding system of the NE and S rifts as revealed by the bilateral 2002/2003 eruptive event at Mt. Etna (Sicily, Italy). Bull. Volcanol. 74 (10), 2415–2433.
Glazner, A.F., Carl, B.S., Coleman, D.S., Miller, J.S., Bartley, J.M., 2008. Chemical Variability and the Composite nature of Dikes from the Jurassic Independence Dike Swarm. eastern California.
Graue, B., Siegesmund, S., Middendorf, B., 2011. Quality assessment of replacement stones for the Cologne Cathedral: mineralogical and petrophysical requirements. Environ. Earth Sci. 63, 1799–1822.
Greiner, S.H., Burchardt, S., Sigmundsson, F., Óskarsson, B.V., Galland, O., Geirsson, H., Rhodes, E., 2023. Interaction between propagating basaltic dikes and pre-existing fractures: a case study in hyaloclastite from Dyrfjöll, Iceland. J. Volcanol. Geoth. Res. 442, 107891.
Greiner, S.H., Galland, O., Sigmundsson, F., Burchardt, S., Geirsson, H., Pedersen, R., Wen, X., 2025. The influence of variable host rock cohesion and magma viscosity on intrusion-fault interaction: insights from laboratory models. J. Geophys. Res. Solid Earth 130 (4), e2024JB029870.
Gretener, P.E., 1969. On the mechanics of the intrusion of sills. Can. J. Earth Sci. 6 (6), 1415–1419.
Groppelli, G., Tibaldi, A., 1999. Control of rock rheology on deformation style and slip-rate along the active Pernicana Fault, Mt. Etna, Italy. Tectonophysics 305 (4), 521–537.
Grosfils, E.B., 2007. Magma reservoir failure on the terrestrial planets: assessing the importance of gravitational loading in simple elastic models. J. Volcanol. Geoth. Res. 166 (2), 47–75.
Gudmundsson, A., 1984. Formation of dykes, feeder-dykes, and the intrusion of dykes from magma chambers. Bull. Volcanol. 47, 537–550.
Gudmundsson, A., 1986. Mechanical aspects of postglacial volcanism and tectonics of the Reykjanes Peninsula, southwest Iceland. J. Geophys. Res. Solid Earth 91 (B12), 12711–12721.
Gudmundsson, A., 2003. Surface stresses associated with arrested dykes in rift zones. Bull. Volcanol. 65 (8), 606–619.
Gudmundsson, A., 2011. Rock Fractures in Geological Processes. Cambridge University Press.
Gudmundsson, A., 2022. The propagation paths of fluid-driven fractures in layered and faulted rocks. Geol. Mag. 159 (11–12), 1978–2001.
Gudmundsson, A., 2025. Multiple dikes make eruptions easy. J. Volcanol. Geoth. Res. 460, 108284.
Guest, J.E., Wood, C., Greeley, R., 1984. Lava tubes, terraces and megatumuli on the 1614–24 pahoehoe lava flow field, Mount Etna, Sicily. Bull. Volcanol. 47 (3), 635–648.
Harp, A., Valentine, G., 2018. Emplacement controls for the basaltic-andesitic radial dikes of Summer Coon volcano and implications for flank vents at stratovolcanoes. Bull. Volcanol. 80, 1–20.
Haimson, B.C., Rummel, F., 1982. Hydrofracturing stress measurements in the Iceland research drilling project drill hole at Reydarfjordur, Iceland. J. Geophys. Res. Solid Earth 87 (B8), 6631–6649.
Hubbert, M.K., Willis, D.G., 1957. Mechanics of hydraulic fracturing. Transactions of the AIME 210 (1), 153–168.
Jolly, R., Sanderson, D., 1997. A Mohr circle construction for the opening of a pre-existing fracture. J. Struct. Geol. 19, 887–892. https://doi.org/10.1016/S0191-8141(97)00014-X.
Kieffer, G., 1975. SUR L'EXISTENCE D'UNE" RIFT ZONE" A L'ETNA (SICILE).
La Sicilia, 1947. In: Sanfilippo, Domenico (Ed.), Issues of 26 February. p. 1. Catania, Italy.
Lamarche, J., Chabani, A., Gauthier, B.D., 2018. Dimensional threshold for fracture linkage and hooking. J. Struct. Geol. 108, 171–179.
Le Corvec, N., Menand, T., Lindsay, J., 2013. Interaction of ascending magma with pre-existing crustal fractures in monogenetic basaltic volcanism: an experimental approach. J. Geophys. Res. Solid Earth 118 (3), 968–984.
Lister, J.R., Kerr, R.C., 1991. Fluid-mechanical models of crack propagation and their application to magma transport in dykes. J. Geophys. Res. Solid Earth 96, 10049–10077. https://doi.org/10.1029/91JB00600.
Maccaferri, F., Acocella, V., Rivalta, E., 2015. How the differential load induced by normal fault scarps controls the distribution of monogenic volcanism. Geophys. Res. Lett. 42 (18), 7507–7512.
Maccaferri, F., Bonafede, M., Rivalta, E., 2010. A numerical model of dyke propagation in layered elastic media. Geophys. J. Int. 180 (3), 1107–1123.
Maccaferri, F., Bonafede, M., Rivalta, E., 2011. A quantitative study of the mechanisms governing dike propagation, dike arrest and sill formation. J. Volcanol. Geoth. Res. 208 (1–2), 39–50.
Maccaferri, F., Rivalta, E., Passarelli, L., Aoki, Y., 2016. On the mechanisms governing dike arrest: insight from the 2000 Miyakejima dike injection. Earth Planet Sci. Lett. 434, 64–74.
Maccaferri, F., Smittarello, D., Pinel, V., Cayol, V., 2019. On the propagation path of magma-filled dikes and hydrofractures: the competition between external stress, internal pressure, and crack length. G-cubed 20 (4), 2064–2081.
Martínez-Poza, A., Druguet, E., Castano, L., Carreras, J., 2014. Dyke intrusion into a pre-existing joint network: the Aiguablava lamprophyre dyke swarm (Catalan Coastal Ranges). Tectonophysics 630, 75–90. https://doi.org/10.1016/j.tecto.2014.05.015.
Mazzarini, F., Armienti, P., 2001. Flank cones at Mount Etna Volcano: do they have a power-law distribution? Bull. Volcanol. 62 (6), 420–430.
Monaco, C., Catalano, S., Cocina, O., De Guidi, G., Ferlito, C., Gresta, S., et al., 2005. Tectonic control on the eruptive dynamics at Mt. Etna Volcano (Sicily) during the 2001 and 2002–2003 eruptions. J. Volcanol. Geoth. Res. 144 (1–4), 211–233.
Monaco, C., Tapponnier, P., Tortorici, L., Gillot, P.Y., 1997. Late Quaternary slip rates on the Acireale-Piedimonte normal faults and tectonic origin of Mt. Etna (Sicily). Earth Planet Sci. Lett. 147 (1–4), 125–139.
Muller, J.R., Ito, G., Martel, S.J., 2001. Effects of volcano loading on dike propagation in an elastic half-space. J. Geophys. Res. Solid Earth 106 (B6), 11101–11113.
Neri, M., Acocella, V., Behncke, B., 2004. The role of the Pernicana Fault System in the spreading of Mt. Etna (Italy) during the 2002–2003 eruption. Bull. Volcanol. 66 (5), 417–430.
Okada, Y., 1985. Surface deformation due to shear and tensile faults in a half-space. Bull. Seismol. Soc. Am. 75, 1135–1154. https://doi.org/10.1785/BSSA0750041135.
Okada, Y., 1992. Internal deformation due to shear and tensile faults in a half-space. Bull. Seismol. Soc. Am. 82, 1018–1040. https://doi.org/10.1785/BSSA0820021018.
Pappalardo, G., Punturo, R., Mineo, S., Contrafatto, L., 2017. The role of porosity on the engineering geological properties of 1669 lavas from Mount Etna. Eng. Geol. 221, 16–28.
Paquet, F., Dauteuil, O., Hallot, E., Moreau, F., 2007. Tectonics and magma dynamics coupling in a dyke swarm of Iceland. J. Struct. Geol. 29 (9), 1477–1493.
Pedicini, M., Bonali, F.L., Corti, N., Pasquaré Mariotto, F.A., Drymoni, K., Tibaldi, A., 2023. A step forward to understanding the development of volcanotectonic rifts: the structure of the Fremrinamar Fissure Swarm (Iceland). Front. Earth Sci. 11, 1271721.

Pedicini, M., Bonali, F.L., Corti, N., Tibaldi, A., 2025. Rift structure and development: the Krafla Fissure Swarm (Northern Iceland). J. Struct. Geol. 191, 105332.
Perras, M.A., Diederichs, M.S., 2014. A review of the tensile strength of rock: concepts and testing. Geotech. Geol. Eng. 32, 525–546.
Philipp, S.L., Afşar, F., Gudmundsson, A., 2013. Effects of mechanical layering on hydrofracture emplacement and fluid transport in reservoirs. Front. Earth Sci. 1, 4.
Ponte, G., 1947. L'eruzione etnea del Febbraio 1947 e le vicende dell'Istituto Vulcanologico dell'Università di Catania. L'Universo 27, 1–9.
Ponte, G., 1948. L'eruzione dell'Etna del febbraio-marzo 1947. Ann. Geofisc. I. . N. I, 1948.
Poppe, S., Galland, O., de Winter, N., Goderis, S., Claeys, P., Debaille, V., Boulvais, P., Kervyn, M., 2020. Structural and geochemical interactions between magma and sedimentary host rock: the Hovedøya case, Oslo Rift, Norway. G-cubed 21, e2019GC008685. https://doi.org/10.1029/2019GC008685.
Proietti, C., De Beni, E., Cantarero, M., Civico, R., Palano, M., Paratore, M., Massaro, G. (2023,. December). 150 years of Etna Summit Craters through a photogrammetry-based time machine. AGU Fall Meeting Abstracts (Vol. 2023, No. 151, V13D–V13D0151.
Rittman, A., 1973. Mount Etna and the 1971 eruption-Structure and evolution of Mount Etna. Phil. Trans. Roy. Soc. Lond. Math. Phys. Sci. 274 (1238), 5–16.
Rivalta, E., Taisne, B., Bunger, A.P., Katz, R.F., 2015. A review of mechanical models of dike propagation: schools of thought, results and future directions. Tectonophysics 638, 1–42.
Rubin, A.M., 1993. Tensile fracture of rock at high confining pressure: implications for dike propagation. J. Geophys. Res. Solid Earth 98, 15919–15935. https://doi.org/10.1029/93JB01391.
Rubin, A.M., 1995. Propagation of magma-filled cracks. Annu. Rev. Earth Planet Sci. 23, 287–336.
Rust, D., Neri, M., 1996. The boundaries of large-scale collapse on the flanks of Mount Etna, Sicily. Geological Society, London, Special Publications 110 (1), 193–208.
Schmiedel, T., Burchardt, S., Mattsson, T., Guldstrand, F., Galland, O., Palma, J.O., Skogby, H., 2021. Emplacement and segment geometry of large, high-viscosity magmatic sheets. Minerals 11. https://doi.org/10.3390/min11101113.
Schultz, R., 1995. Limits on strength and deformation properties of jointed basaltic rock masses. Rock Mech. Rock Eng. 28 (1), 1–15.
Sigmundsson, F., Hooper, A., Hreinsdóttir, S., Vogfjord, K.S., Ofeigsson, B.G., Heimisson, E.R., Dumont, S., Parks, M., Spaans, K., Gudmundsson, G.B., Drouin, V., Arnadottir, T., Jonsdottir, K., Gudmundsson, M.T., Hognadottir, T., Fridriksdottir, H.M., Hensch, M., Einarsson, P., Magnússon, E., Samsonov, S., Brandsdottir, B., White, R.S., Agústsdottir, T., Greenfield, T., Green, R.G., Hjartardottir, A.R., Pedersen, R., Bennett, R.A., Geirsson, H., La Femina, P.C., Bjornsson, H., Palsson, F., Sturkell, E., Bean, C.J., M¨ ollhoff, M., Braiden, A.K., Eibl, E.P.S., 2015. Segmented lateral dyke growth in a rifting event at B´ arðarbunga volcanic system, Iceland. Nature 517, 191–195. https://doi.org/10.1038/nature14111.
Silvestri, S.C., 1949. L'eruzione dell'Etna del 1947. Bull. Volcanol. 9 (1), 81–111.
Sneddon, I.N., 1946. The distribution of stress in the neighbourhood of a crack in an elastic solid. Proc. Roy. Soc. Lond. Math. Phys. Sci. 187 (1009), 229–260.
Spacapan, J.B., Galland, O., Leanza, H.A., Planke, S., 2016. Control of strike-slip fault on dyke emplacement and morphology. J. Geol. Soc. 173, 573–576. https://doi.org/10.1144/jgs2015-166.
Spence, D.A., Turcotte, D.L., 1985. Magma-driven propagation of cracks. J. Geophys. Res. 90, 575–580.
Stephens, T.L., Walker, R.J., Healy, D., Bubeck, A., England, R.W., 2018. Mechanical models to estimate the paleostress state from igneous intrusions. Solid Earth 9, 847–858. https://doi.org/10.5194/se-9-847-2018.
Tibaldi, A., 1995. Morphology of pyroclastic cones and tectonics. J. Geophys. Res. Solid Earth 100 (B12), 24521–24535.
Tibaldi, A., Groppelli, G., 2002. Volcano-tectonic activity along structures of the unstable NE flank of Mt. Etna (Italy) and their possible origin. J. Volcanol. Geoth. Res. 115 (3–4), 277–302.
Tibaldi, A., Bonali, F.L., Pasquaré, F.A., Rust, D., Cavallo, A., D'urso, A., 2013. Structure of regional dykes and local cone sheets in the Midhyrna-Lysuskard area, Snaefellsnes Peninsula (NW Iceland). Bull. Volcanol. 75 (11), 764.
Tibaldi, A., Corti, N., De Beni, E., Bonali, F.L., Falsaperla, S., Langer, H., et al., 2021. Mapping and evaluating kinematics and the stress and strain field at active faults and fissures: a comparison between field and drone data at the NE rift, Mt Etna (Italy). Solid Earth 12 (4), 801–816.
Tibaldi, A., Luppino, A., De Beni, E., Corti, N., Cantarero, M., Mariotto, F.P., Bonali, F.L., 2025. Effects of lateral dyke propagation and pre-existing fractures on shallow deformation: data from the Etna 1947 eruption and analogue models. J. Volcanol. Geoth. Res. 108349.
Tringali, G., Bella, D., Livio, F., Ferrario, M.F., Groppelli, G., Pettinato, R., Michetti, A.M., 2023. Aseismic creep and gravitational sliding on the lower eastern flank of Mt. Etna: insights from the 2002 and 2022 fault rupture events between Santa Venerina and Santa Tecla. Tectonophysics 856, 229829.
Watanabe, T., Masuyama, T., Nagaoka, K., Tahara, T., 2002. Analog experiments on magma-filled cracks: competition between external stresses and internal pressure. Earth Planets Space 54 (12), 1247–1261.
Wauthier, C., Cayol, V., Kervyn, F., d'Oreye, N., 2012. Magma sources involved in the 2002 Nyiragongo eruption, as inferred from an Insar analysis. J. Geophys. Res. Solid Earth 117. https://doi.org/10.1029/2011JB008257.
Wright, T.J., Ebinger, C., Biggs, J., Ayele, A., Yirgu, G., Keir, D., Stork, A., 2006. Magma-maintained rift segmentation at continental rupture in the 2005 Afar dyking episode. Nature 442, 291–294. https://doi.org/10.1038/nature04978.